Thermal desorption mercury records across British Rhaetian–Hettangian sections: Implications for the sedimentary Hg paleovolcanism proxy

Jos Buffington

July 2026

Abstract

Sedimentary mercury is a widely used proxy for reconstructing volcanic emissions from large igneous provinces (LIPs), however, the validity of Hg/TOC normalization relies on several assumptions about host-phase dominance and speciation stability that are rarely tested at the sample level. This study integrates bulk geochemistry, thermal desorption profiles (TDPs), and residual mercury analysis across four late-Triassic to early-Jurassic sections in two sedimentary basins of the British Isles—the Wilkesley borehole, Watchet outcrop, Lavernock Point, and St Audries Bay—to constrain syn- and post-depositional controls on mercury speciation during the end-Triassic mass extinction, which has been attributed to emplacement of the Central Atlantic Magmatic Province (CAMP). Residual mercury trends show divergence among sites, revealing limitations to the use of residual mercury in these British T–J basin settings for quantifying CAMP fluxes. TDP shape data further indicate that Hg-receptor behavior varies with depositional and stratigraphic context. These results show that local sedimentary hosting and preservation can substantially modify bulk Hg records and that TDPs provide an additional diagnostic tool for determining whether Hg/TOC or residual-Hg interpretations are influenced by changes in the sedimentary receptor.

Contents

1 Introduction **4**

1.1 Constraining T–J boundary LIP fluxes 4

1.2 Sedimentary Hg proxy for paleovolcanism 4

1.3 Hg analysis approach for UK Rhaetian–Hettangian sections 5

2 Geologic setting and sites **5**

2.1 Geologic setting 5

2.1.1 Mercia Mudstone Group – Blue Anchor Formation 7

2.1.2 Penarth Group – Westbury Formation 8

2.1.3 Penarth Group – Lilstock Formation – Cotham Member 9

2.1.4 Penarth Group – Lilstock Formation – Langport Member 10

2.1.5 Lias Group – Blue Lias Formation 10

2.2 Study sites . . . 11
2.2.1 Wilkesley core, Cheshire Basin . . . 11
2.2.2 Watchet, Bristol Channel Basin . . . 11
2.2.3 Lavernock Point, Bristol Channel Basin . . . 11
2.2.4 St Audries Bay, Bristol Channel Basin . . . 11

3 Methods **12**
3.1 Sample collection and preparation . . . 12
3.2 Hg concentrations, duplicate treatment, and TDP processing . . . 12
3.3 Stratigraphy and functional lithology . . . 12
3.4 Rolling Hg–TOC and Hg–CaCO3 correlations . . . 13
3.5 Standard tanh–TOC residual Hg . . . 13
3.6 Preservation-aware residual Hg . . . 13

4 Results **15**
4.1 Stratigraphic columns . . . 15
4.1.1 Wilkesley borehole . . . 15
4.1.2 Watchet outcrop . . . 16
4.1.3 Lavernock Point . . . 17
4.1.4 St Audries Bay . . . 18
4.2 Rolling-window Hg–TOC and Hg–CaCO3 correlations . . . 19
4.2.1 TOC correlations . . . 19
4.2.2 CaCO3 correlations . . . 20
4.3 TDP characteristics . . . 21
4.3.1 Site-level TDP distributions . . . 21
4.3.2 Formation-level patterns . . . 22
4.3.3 Lithological controls . . . 23
4.4 Associations between Hg fractions and potential host-phase proxies . . . 26
4.4.1 Wilkesley . . . 26
4.4.2 Watchet . . . 26
4.4.3 Lavernock Point . . . 27
4.4.4 St Audries Bay . . . 27
4.5 Residual mercury across sites . . . 27

5 Discussion **27**
5.1 Hg/TOC cohesion across sites . . . 27

5.2 Limitations to residual Hg for British T–J sections 30
5.3 Insights gained from TDPs 31
5.4 A possible clay-transformation control on early Hg release 32

6 Conclusions **32**

7 References **34**

1 Introduction

1.1 Constraining T–J boundary LIP fluxes

Large igneous provinces (LIPs) represent the largest known volcanic events in Earth's history and have been associated with dramatic perturbations to the global carbon cycle, ocean chemistry, and biosphere. LIP-associated CO_2 emissions have been invoked as primary drivers of mass extinctions and ocean anoxic events across deep time (e.g. Clapham and Renne, 2019). One such event, the end-Triassic mass extinction (ETE), eliminated roughly 50% of marine genera and devastated life on land. This crisis, one of Raup and Sepkoski's (1982) five major mass extinctions, is attributed to emplacement of the Central Atlantic Magmatic Province (CAMP) (e.g. Capriolo et al., 2022). Following the ETE, the Early Jurassic witnessed the initial rifting of Pangea, the opening of the Atlantic Ocean (e.g. Torsvik and Cocks, 2017), and the diversification of marine phytoplankton communities that accelerated transfer of primary production to higher trophic levels (Knoll and Follows, 2016)—events that marked the emergence of the modern Earth system. Quantifying LIP volatile fluxes from sedimentary records is a central challenge in reconstructing carbon-cycle dynamics across Earth history.

CAMP was a sub-aerial LIP with an approximate volume of 2×10^6 km^3 emplaced in the center of the supercontinent Pangea. Its most active period lasted approximately 1 Myr in 3–4 pulses (Marzoli et al., 2004; Blackburn et al., 2013), and intrusive activity preceded extrusive activity (Davies et al., 2017). Negative carbon isotope excursions (CIEs) are common in T–J boundary bulk-organic-carbon isotope records. The characteristic CIE geometry originally described at St Audries Bay contains a 'precursor,' 'initial,' and 'main' CIE and has been correlated across sections globally (Hesselbo et al., 2002; Ruhl and Kürschner, 2011). The same stratigraphic interval contains evidence for ocean acidification (Hautmann et al., 2008; Greene et al., 2012), ocean anoxia (Singh et al., 2023; Richoz et al., 2012), and destabilization of the terrestrial biosphere (Fox et al., 2022; Lindström, 2016). These processes are among the proposed proximate effects of CAMP associated with the ETE. However, despite synchrony among CIEs, CAMP activity, and records of environmental change, variation in the nature, size, and stratigraphic position of CIEs creates uncertainty in exactly how CAMP activity contributed to the temporal development of the extinction (Lindström et al., 2017). The causal relationship between CAMP and the proximate causes of the ETE remains a topic of active discussion (Bond and Grasby, 2017).

1.2 Sedimentary Hg proxy for paleovolcanism

Sedimentary mercury is a leading proxy for paleovolcanism. During eruptions, crustal Hg is volatilized and injected into the atmosphere, where it persists for up to 2 years and can be dispersed globally (Lyman et al., 2020). Mercury is then scavenged from the atmosphere by vegetation and precipitation and incorporated into sediments, commonly through association with organic matter. Anomalous Hg enrichments are therefore used as a proxy for LIPs because volcanic Hg can be transported beyond the immediate volcanic region (e.g. Jiskra et al., 2021). Hg/TOC is the most widely utilized normalization approach, but it is most defensible where organic matter is a dominant Hg host and the background relationship between Hg and TOC is sufficiently stable to support the normalization (Fendley et al., 2024).

Mercury is also scavenged by sulfide minerals, clay minerals, and other phases whose relative contributions vary with depositional environment and redox state (e.g. Bian et al., 2024; Frieling et al., 2024). If multiple host phases contribute significantly to bulk Hg, simple normalization to TOC can be distorted by changing host-phase abundance or dilution. Additional complications include carbonate or siliciclastic dilution (Fendley et al., 2024), non-volcanic Hg sources (Bos et al., 2024), and post-depositional redistribution of Hg (Shen et al., 2020). Mercury speciation can also change during burial

and thermal maturation, with a general tendency toward more thermally stable forms (Indraswari et al., 2025); syn-depositional factors such as kerogen type may influence this trajectory (Liu et al., 2022), and substantial variability in Hg speciation can occur even within the same broad lithologies (Frieling et al., 2024).

Two recently developed analytical approaches help address these limitations. Residual mercury analysis models background relationships between Hg and potential host phases and evaluates Hg remaining above that modeled background (Fendley et al., 2024). Thermal desorption profiles (TDPs) complement this approach by providing sample-level information on the timing and distribution of Hg release during heating. TDPs are rapid, require little sample preparation, and detect Hg at ppb concentrations. In this study, TDPs are divided operationally into Hg_{LT}, released from the beginning of the run through 50 s, and Hg_{HT}, released after 50 s. These fractions constrain differences in thermal stability and binding environment but are not assumed to correspond uniquely to organic-bound Hg, sulfides, clays, cinnabar, or any other single chemical or mineral species (Frieling et al., 2024).

These approaches can identify host-phase or preservation changes that complicate bulk Hg/TOC records. Their importance extends beyond identifying LIP events. Residual-Hg estimates of KFLIP CO_2 emissions from the Mochras core, when incorporated into carbon-cycle box models, produced warming below that inferred from temperature proxies (Fendley et al., 2024). Stow et al. (2026) attributed the discrepancy to additional CO_2 sourced from oxidative weathering of ancient organic carbon, constrained independently using rhenium isotopes. Well-characterized Hg records can therefore contribute to quantitative carbon-flux models, but only where the sedimentary controls on Hg are sufficiently constrained.

1.3 Hg analysis approach for UK Rhaetian–Hettangian sections

Here, this study integrates published, unpublished, and newly collected Hg concentration and TDP data across four upper-Triassic to lower-Jurassic sections in two sedimentary basins of the British Isles: the Wilkesley borehole (Cheshire Basin), the Watchet outcrop at Helwell Bay, St Audries Bay, and Lavernock Point (Bristol Channel Basin). These sites record a range of depositional environments and burial histories, providing an opportunity to separate depositional from post-depositional controls on Hg behavior. My objectives are: (1) identify patterns in Hg speciation as they relate to syn-depositional factors within sites; (2) identify patterns in Hg speciation as they relate to known post-depositional factors across sites; and (3) evaluate whether residual Hg trends are coherent across sites and environments, ultimately clarifying the value of sedimentary Hg for constraining large-scale volcanic carbon fluxes.

2 Geologic setting and sites

2.1 Geologic setting

The studied succession spans the uppermost Triassic to lowermost Jurassic of the United Kingdom. In southwest Britain (Bristol Channel Basin), these strata accumulated in a series of predominantly east–west-trending extensional basins and half-grabens. Major faults generally dipped and downthrew toward the south, producing marked lateral changes in accommodation, water depth, sediment supply, and formation thickness. Palaeozoic basement highs bordered and locally divided the depositional basins, generating proximal, marginal, and more distal marine facies over relatively short distances. The maturity of these Palaeozoic sediments warrants caution when interpreting thermal maturity proxies, including vitrinite reflectance.

Further north, the Cheshire Basin strata were deposited within a depression formed by a complex north–south Permo-Triassic rift system. In this rapidly subsiding segment of the rift, an asymmetrical half-graben preserved more than 4500 m of Permo-Triassic red beds and Jurassic marine strata. Subsequent uplift and basin inversion led to the removal of more than 2000 m of strata, including most of the Jurassic marine sequence (Plant et al., 1999).

Norian environments (predating all studied samples) were commonly restricted, lacustrine, and evaporitic. A major Rhaetian marine transgression progressively established marine conditions across the region. Marine deposition continued through the Triassic–Jurassic transition and into the Early Jurassic. The regional vertical succession records restricted continental or marginal-marine deposition; initial shallow-marine transgression; offshore Westbury mudstone deposition; Cotham shallowing, exposure, and renewed transgression; establishment and drowning of a Langport carbonate ramp; and deposition of cyclic Blue Lias marine mudstone, marl, shale, and limestone.

The succession is highly sensitive to relative sea-level change, making depositional environment an important control on organic matter, carbonate, clay mineralogy, and potential mercury host phases.

These sites have been demonstrated to show largely negligible differences in burial history and as a result, thermal maturity. The burial history of the Bristol Channel Basin was more recently examined by Cornford (1986). This study examined the carbon-preference indices, pristane/phytane ratios, and vitrinite reflectance values between Lavernock point and Doniford Bay (closest to St Audries Bay and Watchet). The resulting estimates in burial depth placed Lavernock Point only a few hundred meters deeper than Doniford Bay at its maximum burial. A relatively high vitrinite reflectance from St Audries Bay (0.8 - 1.1%) published by Kaiho et al. (2022) might be explained by residual organic matter from the basin's thermally mature Paleozoic parent material. Wilkesley in the Cheshire Basin was found to have a mean Tmax just over 435* C. When compared with the work of Indraswari et al. (2024) on the Lower Saxony Basin, these sites are similar to the lowest maturity core studied. Their other cores reached estimated depths/temperatures of 4300 m/200 °C and 5600 m/260 °C. The differences between our sites are closer to between 1 and 2.5 kilometers and, consequently, the burial depth differences can be assumed to have negligible impact on the mercury interpretation.

2.1.1 Mercia Mudstone Group – Blue Anchor Formation

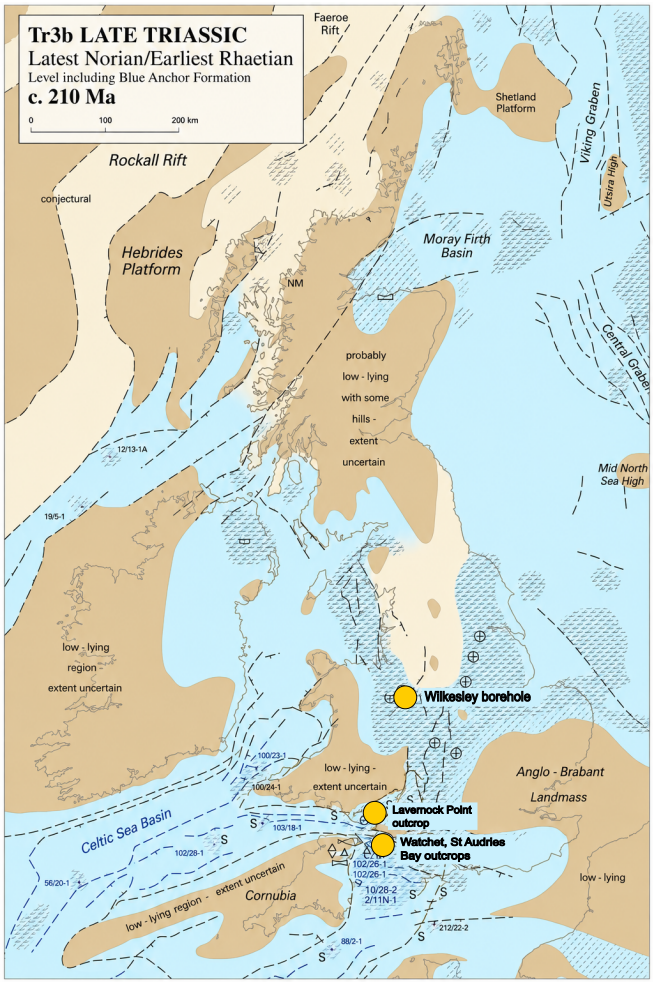

Figure 1: Blue Anchor Paleogeography of Southwest Britain

The Rhaetian Williton Member of the Blue Anchor Formation has its type section at St Audries Bay, where it is approximately 2 m thick. It consists of thinly laminated mudstone and fine-grained sandstone, within a broader Blue Anchor/Mercia succession that also includes marl. Marine trace fossils and bivalves support a shallow-marine interpretation, and the Williton represents the initial Late Triassic marine transgression in southwest Britain (Hesselbo et al., 2004).

2.1.2 Penarth Group – Westbury Formation

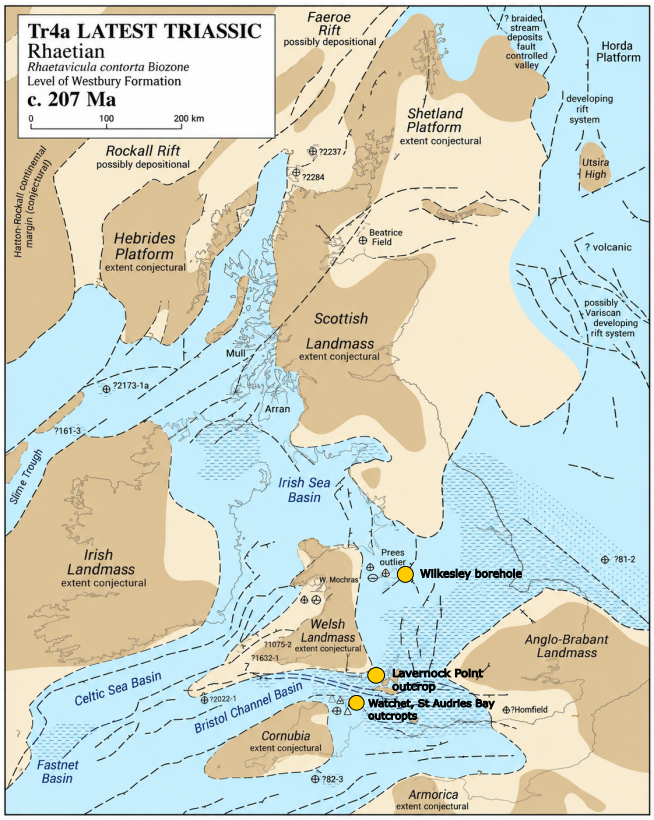

Figure 2: Westbury paleogeography of Southwest Britain

The Westbury Formation forms the lower part of the Penarth Group and is Rhaetian in age. It is a regionally extensive marine unit dominated by mudstone with interstratified siltstone and locally phosphatic conglomerate, sandstone, and carbonate concretions (Hesselbo et al., 2004). At St Audries Bay, carbonate is concentrated in discrete concretionary horizons, probably reflecting post-depositional dissolution because calcitic macrofossils are commonly preserved as empty moulds. Bivalves are common, vertebrate debris occurs especially in the lower part of the formation, and basal or intraformational bone beds have been interpreted as winnowed lags.

The main Westbury succession was deposited in shallow, generally quiet-water offshore conditions, periodically affected by wave-base impingement. It was generally deeper and farther offshore than the underlying Williton Member. The upper Westbury shallows at many localities; this is especially prominent at Lavernock Point and elsewhere in south Wales, where the succession coarsens into prograding shoreface sandstone (Hesselbo et al., 2004).

2.1.3 Penarth Group – Lilstock Formation – Cotham Member

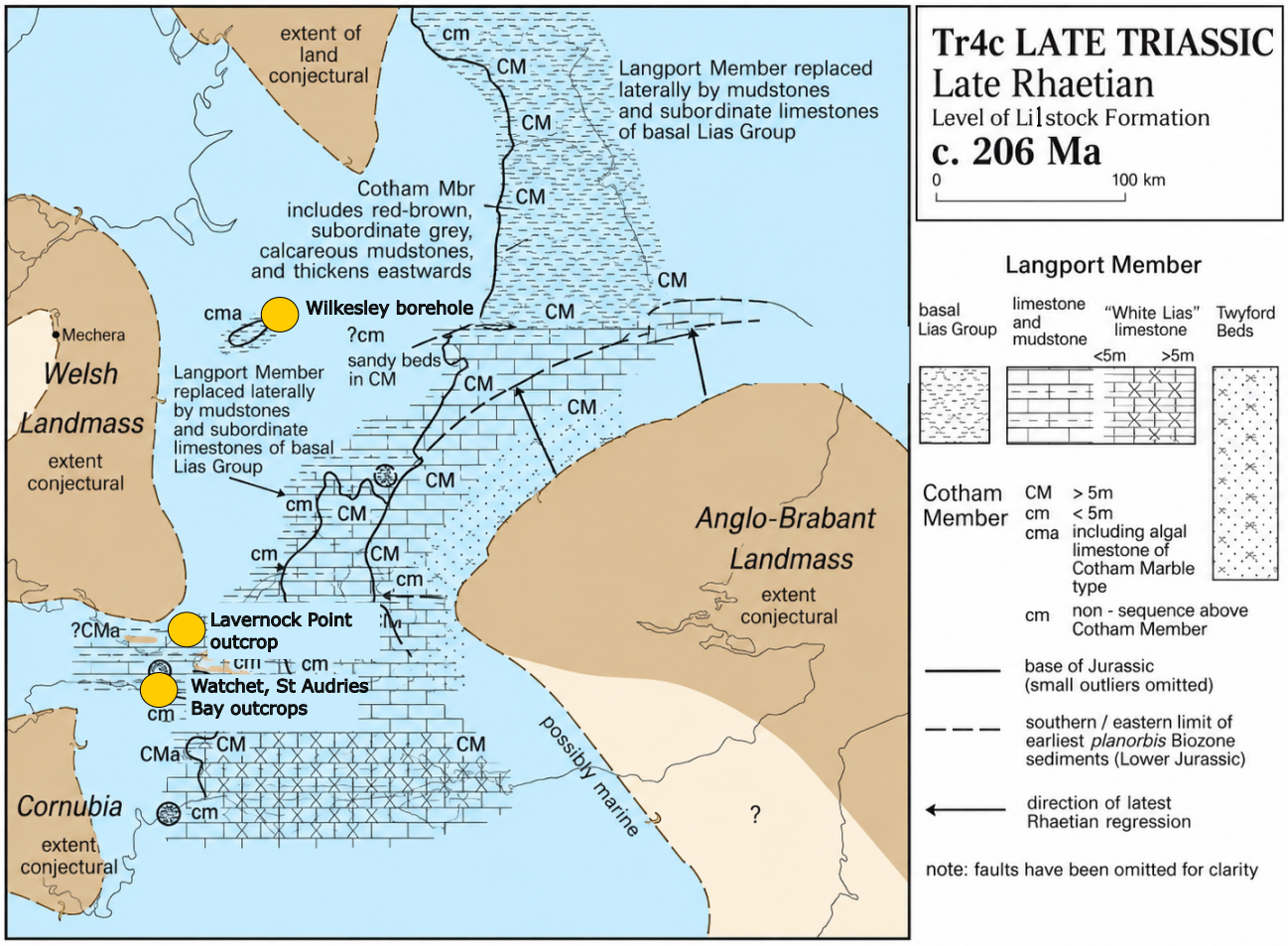

Figure 3: Lilstock paleogeography of Southwest Britain

The Cotham Member is the lower member of the Lilstock Formation. It comprises mudstone, fine-grained sandstone, and limestone and is Rhaetian in age, although assignment of its uppermost part depends on the chosen T–J boundary definition (Hesselbo et al., 2004). The Westbury–Cotham transition is commonly gradational. In the Bristol Channel region, the lower Cotham contains thinly interbedded siltstone and fine-grained sandstone and is interpreted as a shoreface equivalent of more offshore Westbury deposition. Soft-sediment deformation is widespread, producing the characteristic 'deformed bed' or 'slump bed.' Proposed triggers include liquefaction and seismic disturbance.

The lower Cotham shallows upward and is capped by an erosional surface with desiccation cracks extending as much as approximately 90 cm downward at localities including Lavernock Point and St Audries Bay. This surface, often termed the 'intra-Rhaetic unconformity,' records a pronounced relative sea-level fall and brief subaerial exposure. The generally unstratified crack fills indicate a short exposure event rather than repeated long-term desiccation (Hesselbo et al., 2004).

The upper Cotham comprises mudstone, siltstone, and fine-grained calcareous sandstone deposited during renewed relative sea-level rise. Symmetrical and locally flat-topped wave ripples indicate extremely shallow coastal water at some horizons, locally only a few centimeters deep. Radial calcite ooids occur in sandy limestone beds and some crack fills. The Cotham Marble is a prominent carbonate marker near

the top of the member in parts of the Bristol region and contains microbial/stromatolitic components regionally. Microbial textures observed at St Audries Bay and Lavernock Point may nevertheless reflect the same shallow, locally fresh-to-brackish conditions that favor microbial carbonate development, and are treated here as local facies features rather than as a uniform Cotham lithology. Ostracod assemblages include both marine and non-marine forms, which is consistent with strongly fluctuating coastal conditions.

2.1.4 Penarth Group – Lilstock Formation – Langport Member

The Langport Member is the upper member of the Lilstock Formation. Its assignment to the latest Rhaetian or earliest Hettangian depends on the chosen boundary definition. The lower contact with the Cotham Member is sharp but conformable and is interpreted as a flooding surface formed when relative sea-level rise outpaced clastic sediment supply (Hesselbo et al., 2004). The unit was deposited in a fully marine setting and includes pale gray micritic limestone, impure and argillaceous limestone, nodular limestone, calcareous mudstone, and locally siltstone.

Pure pale micritic Langport limestone is traditionally termed the White Lias. Hummocky and swaley cross-stratification records storm influence, and some micritic limestone probably originated as peloidal grainstone before recrystallization. The regional depositional system is interpreted as a carbonate ramp. Local slope development generated downslope transport and gravity-flow deposits, and the ramp geometry may have resulted from depositional buildup, syn-sedimentary tectonic tilting, or a combination of both (Hesselbo et al., 2004).

In west Somerset and south Wales, parts of the Langport are thin and dominated by impure limestone and calcareous mudstone. Hesselbo et al. (2004) interpret such thin successions at St Audries Bay and Lavernock Point as sediment-starved, relatively distal parts of the carbonate-ramp system. The top Langport surface is interpreted as a regional drowning surface marking failure or shutdown of carbonate production during continued relative sea-level rise. This sediment-starved distal-ramp interpretation is also relevant when considering the very thin Langport interval identified at Wilkesley, although that is only evidence for this interpretation.

2.1.5 Lias Group – Blue Lias Formation

The Blue Lias Formation lies at the base of the Lias Group and is principally earliest Jurassic in the studied successions. Typical Blue Lias deposition was fully marine and consists of rhythmic alternations of laminated organic-rich shale, pale and dark marl, mudstone, and limestone. These cycles have been interpreted as fourth- or fifth-order Milankovitch-scale variability, although the specific periodicity remains debated (Hesselbo et al., 2004).

Carbonate was redistributed during diagenesis, producing nodular and concretionary limestones. Bottom-water oxygenation varied substantially: laminated organic-rich shale records intervals of reduced benthic activity and poorer oxygenation, whereas more heavily burrowed marl and limestone record better-oxygenated conditions. The Langport–Blue Lias transition varies regionally, being abrupt in more marginal settings and gradational in more distal settings. In some localities, the lowest Blue Lias limestones resemble the underlying Langport. In the Watchet area, the basal Blue Lias has historically been called the Paper Shale. The Blue Lias records drowning of the Langport carbonate ramp and renewed dominance of deeper-water mixed carbonate–siliciclastic sedimentation (Hesselbo et al., 2004).

2.2 Study sites

2.2.1 Wilkesley core, Cheshire Basin

The Wilkesley borehole (grid reference SJ 363864 341438), near Perthy, Shropshire, was drilled by the British Geological Survey in 1959–1960 to a depth of 1686 m and recovered strata spanning the Early Triassic to Early Jurassic. Legacy core material includes fossil specimens with precise depth information and bulk-rock aggregates retained at approximately one-foot intervals (Ullmann et al., 2026). Triassic–Jurassic boundary samples were collected from these one-foot intervals, and this study adds supplementary sampling from approximately 15 m below to nearly 80 m above the boundary.

The analyzed succession includes: Westbury Formation, Cotham Member of the Lilstock formation, and the Blue Lias Formation. The Westbury Formation is approximately 7.8 m in the sampled region. The Cotham Member overlies the Westbury. A fine-grained argillaceous limestone above the Cotham is interpreted as Langport, and strata above the Langport belong to the Blue Lias. The Langport Member is especially thin at Wilkesley, and no sample from one-foot increments is attributed to it. This is consistent with seidment-starvation that may happen in a distal part of a carbonate-ramp system, as the Langport has been interpretted as before.

2.2.2 Watchet, Bristol Channel Basin

Helwell Bay at Watchet, Somerset (grid reference ST 08090 43418) lies within the Bristol Channel Basin approximately 5 km west of St Audries Bay. The exposure preserves the Rhaetian Westbury and Lilstock formations and the Hettangian Blue Lias Formation. In the Watchet site interpretation, depositional conditions shift from restricted to shallow-marine Westbury deposition through the very shallow, locally peritidal Cotham, to open-marine Langport carbonate-ramp deposition and deeper-water mixed carbonate–siliciclastic Blue Lias sedimentation. Thirty samples were collected from −50 to +475 cm relative to the base of the Cotham Member (Davies, 2025).

2.2.3 Lavernock Point, Bristol Channel Basin

Lavernock Point, situated on the South Wales coast (grid reference ST 18732 68152), exposes a similar Rhaetian–Hettangian succession to Watchet but in a slightly more proximal position within the Bristol Channel Basin. The upper Westbury Formation here is notable for local shallowing and sandstone progradation, representing a more proximal or shoreward upper-Westbury facies than some Somerset sections. There is a "special bed" of microbilite present between the Cotham and Langport Members. The shales in the basal Blue Lias are referred to as the Paper Shales. 74 samples were collected at a varied resolution by Pantazopoulou (2023) 590 cm above and 570 cm below the T-J boundary.

2.2.4 St Audries Bay, Bristol Channel Basin

St Audries Bay lies on the Somerset coast of the Bristol Channel Basin and is one of the most complete and extensively studied southwest-British T–J boundary sections. It contains the most complete formation coverage in this study, including the Blue Anchor Formation (Williton Member), Westbury Formation, Cotham and Langport members of the Lilstock Formation, and Blue Lias Formation. The Williton Member is approximately 2 m thick and records the initial shallow-marine Rhaetian transgression. The Westbury is dark at St Audries Bay but is not particularly organic rich, the section is relatively expanded, and it lacks the prominent basal Westbury bone bed present at many other

localities. Carbonate is concentrated in discrete concretionary horizons (Hesselbo et al., 2004).

The section is notable for its detailed biostratigraphic and carbon-isotope records and was proposed as a candidate Global Stratotype Section and Point for the base of the Jurassic. Most geochemical samples used in the Hesselbo et al. St Audries Bay profile were excavated from the foreshore and described as unweathered. The samples used here were collected by Stephen Hesselbo and Stuart Robinson (Hesselbo et al., 2004) and span approximately 13 m below to 11 m above the T–J boundary.

3 Methods

3.1 Sample collection and preparation

Sample locations, stratigraphic coverage, and original collection procedures are described in Section 2.2. Wilkesley core samples were obtained from the British Geological Survey at approximately one-foot stratigraphic intervals. Samples analyzed during this study were powdered using a Fritsch steel ball mill in the Department of Earth Sciences, University of Oxford

This study combines newly generated Hg and thermal-desorption measurements with previously published or existing geochemical datasets. Additional geochemical data for Wilkesley were taken from Ullmann et al. (2026). Corresponding geochemical datasets for Watchet, Lavernock Point, and St Audries Bay were taken from Davies (2025), Pantazopoulou (2023), and Hesselbo et al. (2004), respectively.

3.2 Hg concentrations, duplicate treatment, and TDP processing

Mercury concentration was analyzed using a Lumex 915Lab with autosampler in the Department of Earth Sciences, University of Oxford. Calibration used paint-contaminated soil reference material NIST 2587, containing 290 ppb (ng/g) Hg. Approximately 200 ± 5 mg of each sample was weighed for analysis.

The analytical run associated with this work included a duplicate approximately every 15 samples; the Davies (2025) Watchet dataset contained four duplicate pairs. Duplicate precision was evaluated using relative percent difference (RPD) for HgT, HgLT, and HgHT, and all tested pairs had RPD $< 20\%$. Duplicate runs representing the same sample were collapsed before downstream TDP analysis. TDP runs for the Lavernock Point and St Audries Bay samples were conducted by Guest (2025).

Total integrated Hg over the shared interval is denoted HgT. HgLT is the integrated Hg released from the beginning of the run through 50 s, and HgHT is the Hg released after 50 s through 213 s, such that

$$HgLT(\%) = 100\frac{HgLT}{HgT}, \qquad HgHT(\%) = 100\frac{HgHT}{HgT}.$$

3.3 Stratigraphy and functional lithology

Lithologic terminology differs substantially among the original site descriptions as each was described by a different set of workers. To permit only broad cross-site comparisons, samples were grouped into three functional lithologies: Mud-rich, Sandstone, and Carbonate. Mud-rich includes mudstone, mudrock, shale, claystone, clay-rich, argillaceous, siltstone, and silty descriptions. Sandstone includes sandstone, sand, and arenitic. Carbonate includes limestone, marl, calcareous carbonate, concretionary carbonate, dolomitic carbonate, chalk, and microbial carbonate. Thus, mixed descriptions such as calcareous

mudstone and muddy carbonate concretion are classified as Mud-rich. The harmonized categories are used only as supplementary analytical groupings and do not replace the original lithologic logs.

3.4 Rolling Hg–TOC and Hg–CaCO3 correlations

To identify the timing of Hg release most strongly associated with organic matter, rolling Pearson r and Spearman ρ correlations were calculated between release rate and bulk TOC using 5, 10, and 20 s windows shifted through the TDP in 1 s increments, following the general approach of Frieling et al. (2024). Correlations were evaluated at whole-site level and within lithostratigraphic units where sample size permitted. An analogous analysis was applied to $CaCO_3$ for Wilkesley, Lavernock Point, and St Audries Bay. Watchet was excluded from the rolling $CaCO_3$ analysis because defensible sample-matched $CaCO_3$ data were unavailable.

3.5 Standard tanh–TOC residual Hg

Standard residual Hg was calculated from both HgT and HgLT using a site-specific nonlinear relationship with bulk TOC, following the saturating approach used by Krishnaswamy et al. (2026) and the general host-correction logic of Fendley et al. (2024). HgLT was selected because the rolling analyses show that early release is generally more closely associated with TOC than later release. Each site was fitted independently over its full available dataset using robust nonlinear regression with `robustbase::nlrob`:

$$\widehat{HgT}_i = a \tanh\left(\frac{TOC_i}{b}\right) + c,$$

$$\widehat{HgLT}_i = a \tanh\left(\frac{TOC_i}{b}\right) + c,$$

where a controls the magnitude of the modeled increase, b controls the TOC scale over which the relationship approaches saturation, and c represents modeled HgLT at low TOC. Robust fitting down-weights large departures so that anomalous samples exert less influence on estimation of the background relationship.

Residual HgLT was calculated as

$$HgR_{LT,i} = HgLT_{i,\text{observed}} - \widehat{HgLT}_i,$$

and expressed both in concentration units and relative to the robust residual standard error (RRSE):

$$HgR_{LT,\text{RRSE}} = \frac{HgR_{LT}}{RRSE}.$$

Positive residuals indicate more HgLT than predicted by the site-specific HgLT–TOC relationship, values near zero are consistent with the fitted background, and negative values indicate less HgLT than predicted. Values above approximately +2 RRSE were treated as statistically unusual positive departures.

3.6 Preservation-aware residual Hg

A secondary preservation-aware workflow tested whether TDP shape explained HgT variability remaining after nonlinear Hg–TOC correction. A robust nonlinear Hg–TOC host background was first fitted

as

$$\widehat{Hg}_{\mathrm{host},i} = a \tanh\left(\frac{TOC_i}{b}\right) + c,$$

and conventional residuals were calculated as

$$r_{i,\mathrm{conv}} = HgT_{i,\mathrm{observed}} - \widehat{Hg}_{\mathrm{host},i}.$$

These residuals were screened separately against two TDP-shape metrics: TDP centroid time and the fraction of Hg released during the first 50 s. The two metrics were not entered together because they are redundant. Where a shape metric improved the host-only model, the standardized metric

$$S_i = \frac{S_i - \overline{S}}{s_S}$$

was added to the modeled background. A pooled preservation-aware model therefore had the general form

$$\widehat{Hg}_i = a \tanh\left(\frac{TOC_i}{b}\right) + dS_i + c.$$

Centroid time is calculated as

$$t_{\mathrm{centroid}} = \frac{\displaystyle\int_0^{213\,\mathrm{s}} t\, r_+(t)\,\mathrm{d}t}{\displaystyle\int_0^{213\,\mathrm{s}} r_+(t)\,\mathrm{d}t}, \qquad r_+(t) = \max[r(t), 0]$$

Formation structure was then tested to determine whether the preservation relationship differed among lithostratigraphic units. Where supported, the final model allowed formation-specific intercepts and TDP slopes:

$$\widehat{Hg}_i = H_i + \alpha + \gamma_{f(i)} + \left[\beta + \eta_{f(i)}\right] S_i,$$

where H_i is the nonlinear Hg–TOC prediction, $\gamma_{f(i)}$ is a formation-specific intercept, and $\eta_{f(i)}$ is a formation-specific preservation slope. Final residual Hg was then

$$HgR_i = HgT_{i,\mathrm{observed}} - \widehat{HgT}_{i,\mathrm{background}}.$$

Multiple near-best nonlinear Hg–TOC fits were propagated rather than selecting one arbitrary tanh solution: host surfaces within 1% of the best robust residual scale were retained, providing an ensemble of plausible modeled backgrounds. Final models were also refitted after low-weight exclusions to test sensitivity to influential observations. Sample-level residual uncertainty was summarized across the near-best surfaces, and stable high residuals were identified where a large majority of near-best solutions remained above the positive anomaly threshold.

The retained model structure was site-specific. Wilkesley used the full carbonate-free analytical basis and retained formation-specific relationships with TDP centroid, with a secondary $CaCO_3$ sensitivity term. St Audries Bay used the bulk analytical basis and retained formation-specific relationships with

the early-release fraction, again with $CaCO_3$ considered as a secondary control. Lavernock Point used the full carbonate-free analytical basis but retained no TDP-shape metric; its selected background comprised the nonlinear Hg–TOC relationship and a common residual offset.

4 Results

4.1 Stratigraphic columns

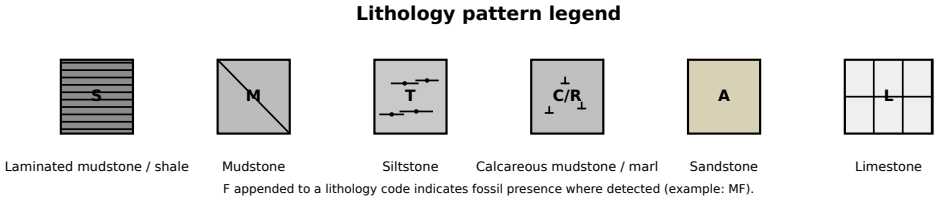

Figure 4: Legend for lithology patterns on lithostratigraphy plots.

The full dataset contains 571 independent samples, grouped functionally as 454 Mud-rich, 29 Sandstone, and 88 Carbonate. Normalized-TDP figures include 570 profiles because the Wilkesley sample taken at 382 feet depth was disrupted by the machine sleeping, and is excluded from unit-area normalization.

4.1.1 Wilkesley borehole

The final Wilkesley stratigraphic dataset (Figure 5) contains 221 samples: 17 Westbury, 17 Cotham, no Langport, and 187 Blue Lias. Wilkesley is substantially more lithologically homogeneous than the Bristol Channel Basin sites and is dominated by mud-rich calcareous mudstone and siltstone, with carbonate beds becoming more common in the Blue Lias. No analyzed sample falls within the very thin Langport interval.

TOC is relatively high and variable in the Westbury, decreases markedly through the Cotham, and increases again across the lower Blue Lias. HgT is highly variable throughout the borehole. The largest absolute HgT concentrations occur in the Westbury, whereas concentrations in the Cotham are generally lower; nevertheless, HgT/TOC increases strongly within the Cotham and produces several of the largest ratio values in the section. Additional HgT/TOC peaks occur immediately above the T–J boundary within the pre-*P. planorbis* Blue Lias, and the ratio remains variable through the rest of the Blue Lias with several isolated excursions. HgLT/TOC broadly reproduces the major Cotham and earliest Blue Lias excursions. The fraction of Hg released as HgLT is generally high in the Westbury and becomes lower and more variable through the Cotham and Blue Lias. $CaCO_3$ is generally low in the Westbury, increases through the Cotham, and becomes highly variable in the Blue Lias. Rb/Zr is comparatively stable through much of the succession but has several localized excursions, including within the Cotham. The $\delta^{13}C$ record is also strongly variable across the upper Rhaetian and lower Hettangian succession, and the conventional ‘precursor,’ ‘initial,’ and ‘main’ CIE geometry used for regional correlation is recognizable in the Wilkesley record.

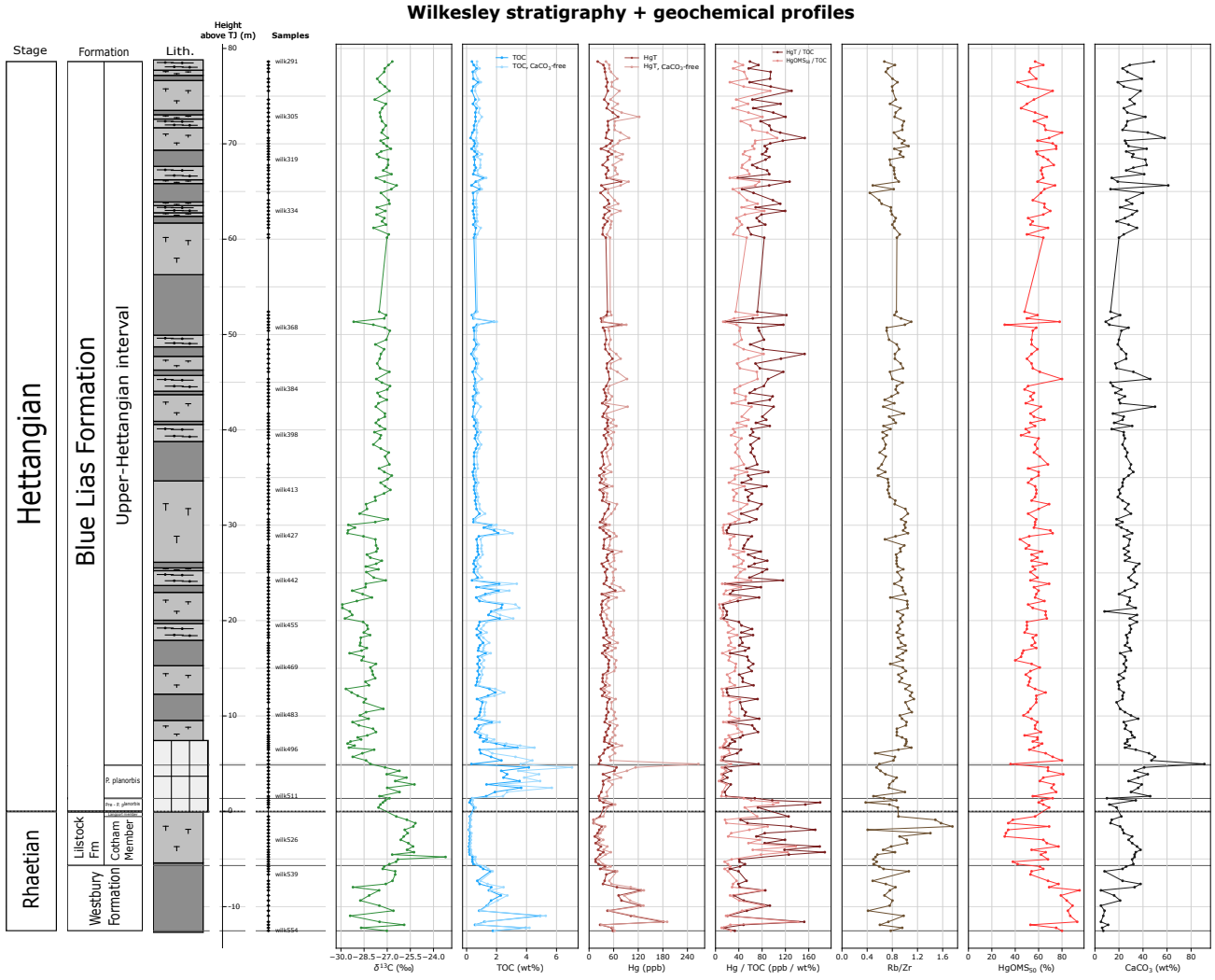

Figure 5: Geochemistry, lithology, and stratigraphy plot for the Wilkesley borehole.

4.1.2 Watchet outcrop

The final Watchet dataset (Figure 6)contains 30 samples: 3 Westbury, 13 Cotham, 7 Langport, and 7 Blue Lias. TOC is moderate in the Westbury and decreases through much of the Cotham and Langport before increasing sharply at the base of the Blue Lias and remaining comparatively high through most of the sampled Blue Lias. The $\delta^{13}C$ record becomes progressively more negative through the upper Cotham and Langport before shifting toward less negative values in the Blue Lias.

HgT is moderately elevated in the Westbury but decreases across the lower Cotham. Several discrete HgT excursions occur in the middle and upper Cotham, and HgT increases again across the transition into the Blue Lias. The largest and most sustained HgT/TOC excursions occur in the middle and upper Cotham; HgLT/TOC follows the same broad pattern and also reaches its largest values there. Both HgT/TOC and HgLT/TOC decrease markedly in the Blue Lias despite the increase in TOC and, in several samples, absolute HgT. The HgLT fraction is variable through the Cotham and Langport and generally reaches higher values in the upper Blue Lias.

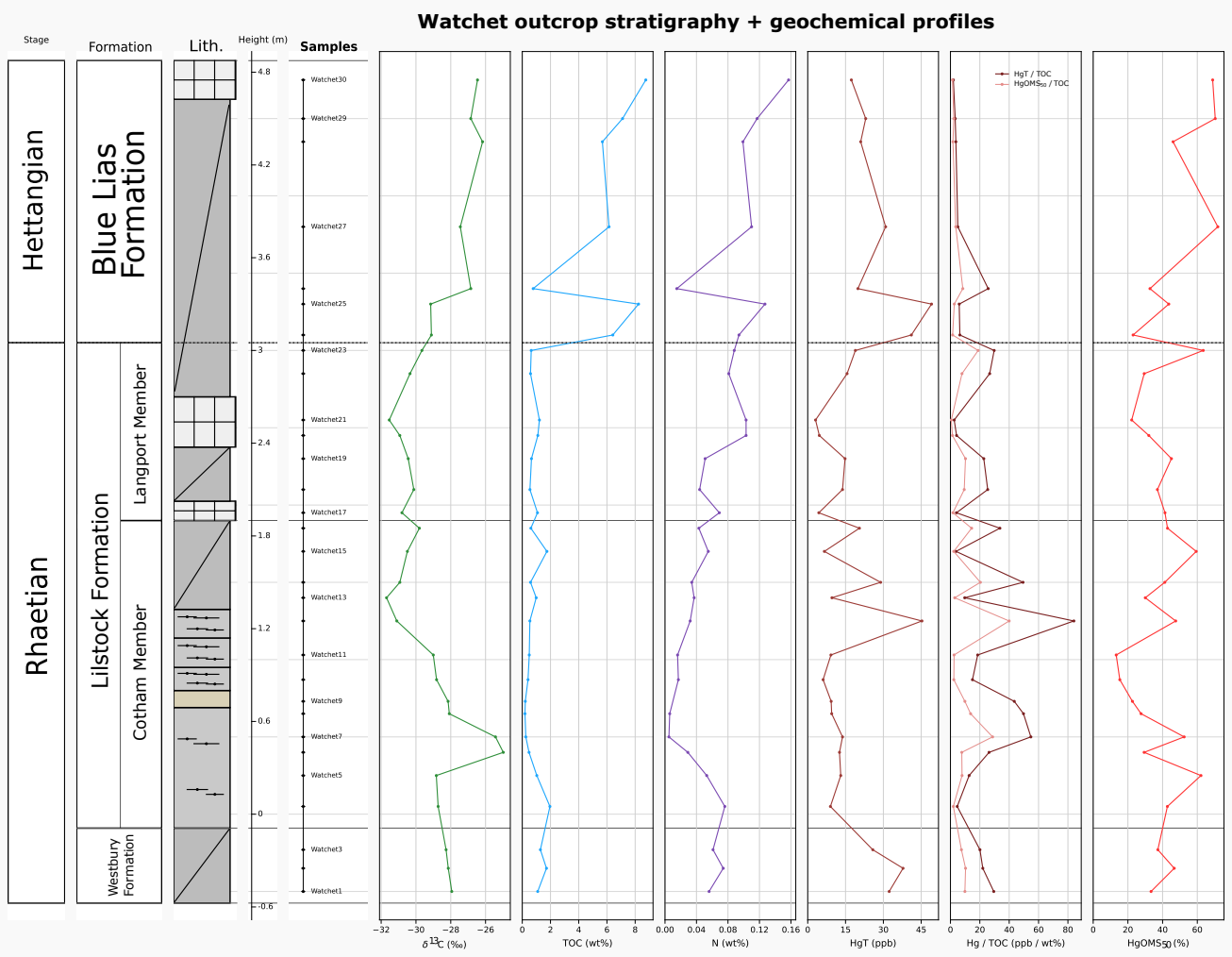

Figure 6: Geochemistry, lithology, and stratigraphy plot for the Watchet outcrop.

4.1.3 Lavernock Point

The final Lavernock Point dataset (Figure 7) contains 74 samples: 7 Westbury, 14 Cotham, 14 Langport, and 39 Blue Lias. TOC is relatively low to moderate through the Westbury, Cotham, and Langport before increasing sharply at the base of the Blue Lias, particularly in the densely sampled basal interval. HgT is moderate through most of the Westbury and lower through much of the Cotham–Langport succession.

A very narrow, pronounced HgT excursion occurs near the top of the Cotham in the interval identified as the 'special bed.' The largest HgT/TOC excursion in the entire Lavernock record occurs in this upper-Cotham interval and is dominated by a single sample. HgT/TOC is nevertheless elevated more broadly across parts of the Cotham and Langport relative to much of the Blue Lias. HgLT/TOC reproduces the narrow special-bed excursion and smaller elevations elsewhere in the Cotham and Langport. Absolute HgT rises markedly at the base of the Blue Lias together with TOC, but HgT/TOC remains comparatively low through much of the Blue Lias. The HgLT fraction is generally lower through the Cotham and Langport and increases across much of the Blue Lias. $CaCO_3$ is low through much of the Westbury and becomes substantially higher and more variable in the Cotham, Langport, and Blue Lias. The $\delta^{13}C$ profile shows a pronounced negative excursion across the upper Cotham–Langport–lower Blue

Lias succession.

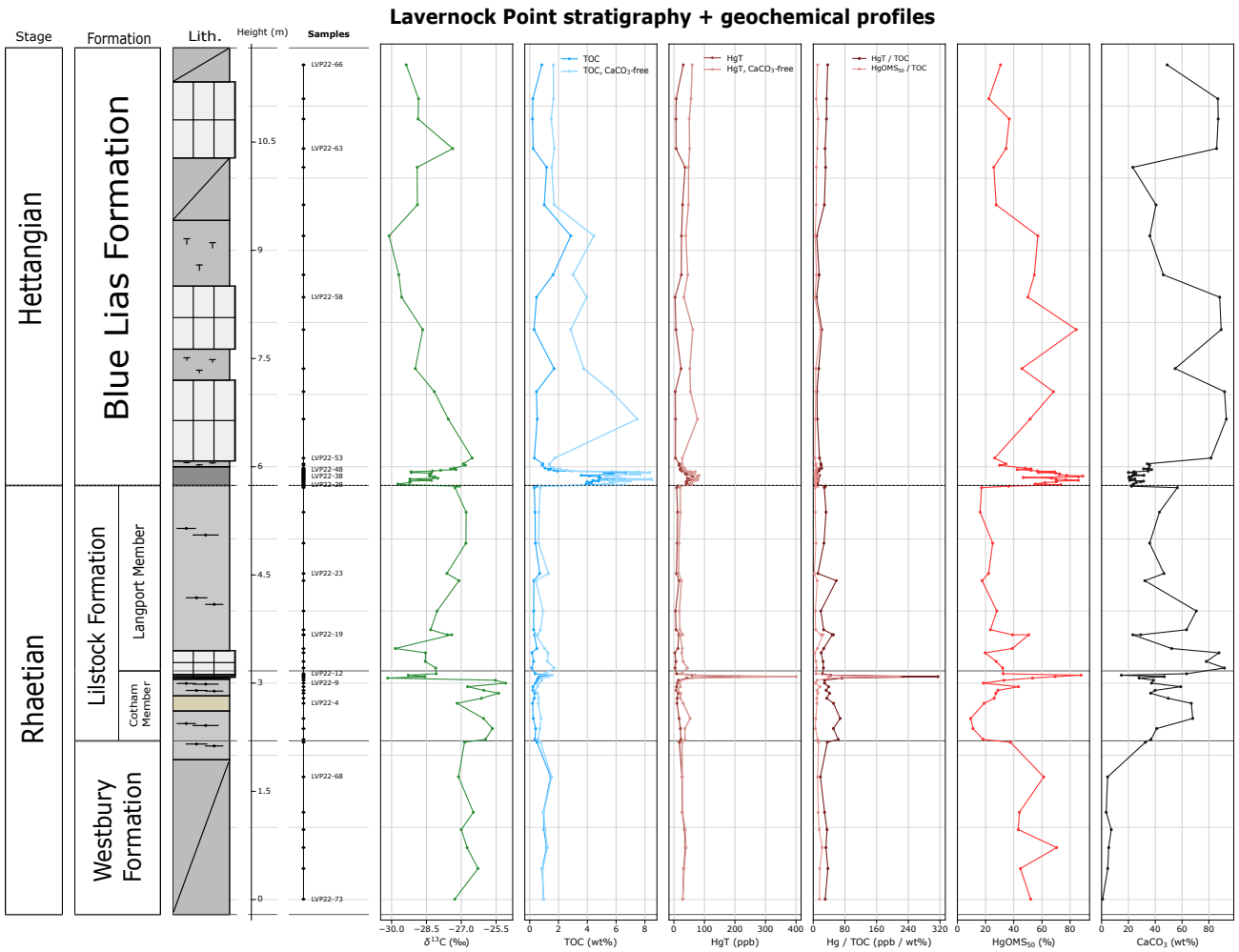

Figure 7: Geochemistry, lithology, and stratigraphy plot for the Lavernock Point outcrop.

4.1.4 St Audries Bay

The final St Audries Bay dataset (Figure 8) contains 246 samples: 24 Blue Anchor, 96 Westbury, 13 Cotham, 11 Langport, and 102 Blue Lias, making it the densest sampled profile in this study. TOC is very low within much of the Blue Anchor, higher and more variable through the Westbury, lower again through the Cotham and Langport, and substantially higher in the Blue Lias.

Several of the largest HgT/TOC values in the lower part of the section occur in the Blue Anchor and coincide with very low TOC. HgT and HgT/TOC remain variable through the Westbury with multiple discrete excursions. The Cotham contains another interval of elevated HgT/TOC, including a pronounced excursion in the middle part of the member, although absolute HgT in the Cotham is generally moderate relative to the highest concentrations elsewhere in the section. HgT and HgT/TOC are generally lower through the Langport, with isolated excursions. Absolute HgT rises substantially in the Blue Lias, where several of the highest HgT concentrations occur, but TOC also increases strongly and HgT/TOC is consequently generally lower than the largest Rhaetian ratio excursions. HgLT/TOC broadly follows the principal HgT/TOC excursions but differs in relative magnitude among units. The HgLT fraction is comparatively high through much of the Westbury, decreases in the Cotham, and

becomes more variable in the Langport and Blue Lias. $CaCO_3$ is generally low through much of the Westbury, rises sharply in the Cotham and Langport, and remains high but variable in the Blue Lias. The $\delta^{13}C$ record shifts toward more negative values across the Langport and into the Blue Lias.

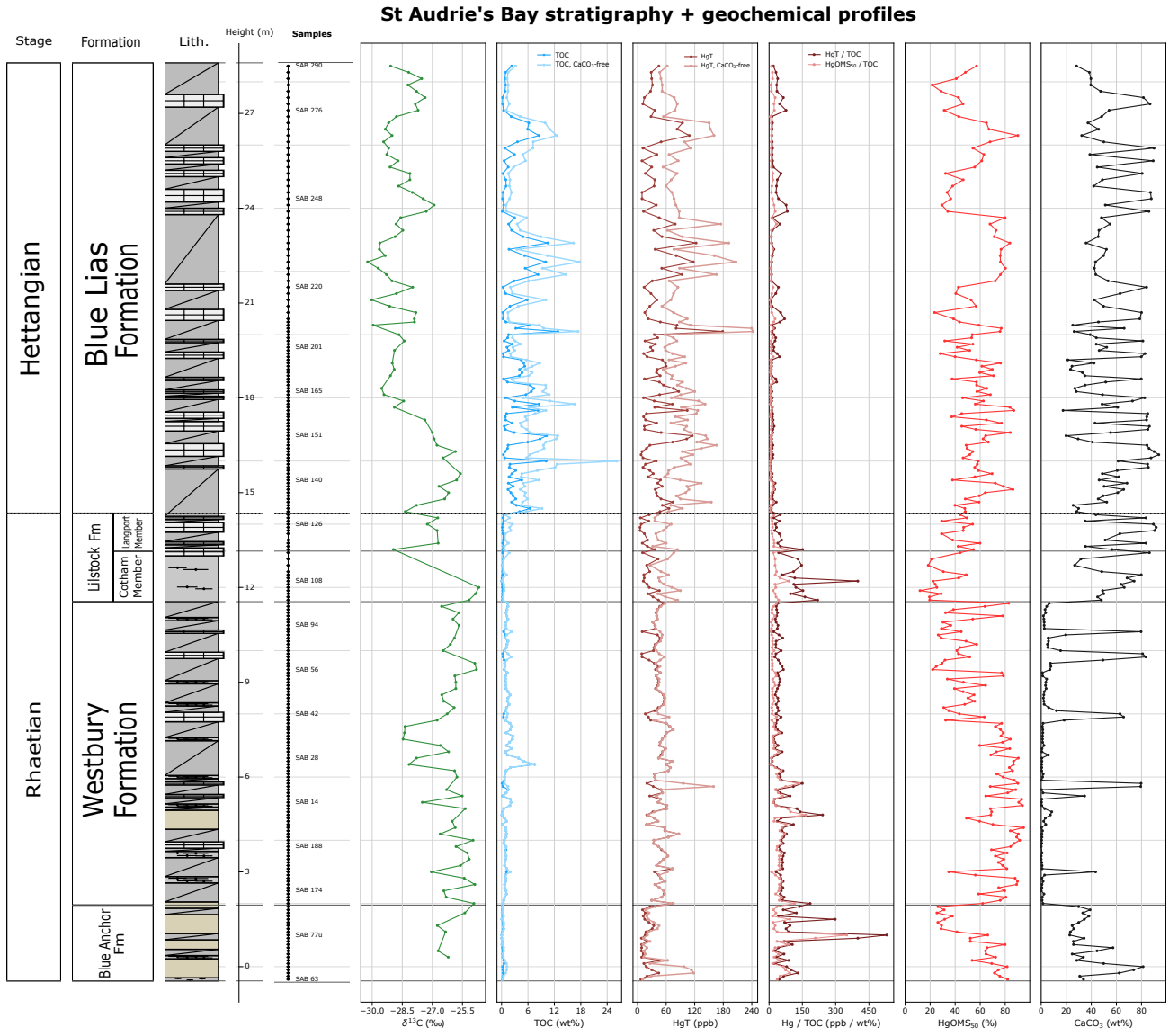

Figure 8: Geochemistry, lithology, and stratigraphy plot for St Audries Bay outcrop.

4.2 Rolling-window Hg–TOC and Hg–CaCO3 correlations

4.2.1 TOC correlations

Across the four sites, Hg–TOC association is generally strongest during the early part of the TDP, but the strength and exact timing vary among sites and formations. Lavernock Point shows the clearest early positive relationship: strong positive correlations occur at whole-site level and in the Blue Lias, then weaken substantially later in the TDP. St Audries Bay similarly shows a broad early positive whole-site relationship, reproduced in several formations and especially clearly in the Blue Lias. Wilkesley is more heterogeneous, with different stratigraphic intervals showing different Hg–TOC relationships,

although positive early correlations remain evident in several intervals including the Cotham and parts of the Hettangian succession. Watchet also shows an early positive whole-site relationship and an early positive Cotham relationship, but formation-level interpretation is less secure because several units have small sample sizes.

The broad early association persists across 5, 10, and 20 s windows, indicating that the TOC-associated signal is not restricted to one narrow time point. Rather, it occupies a broader early-release interval whose exact geometry differs among sites and formations.

Justification for the 50 s operational cutoff The maximum Hg–TOC correlation does not occur at exactly 50 s in every site or formation, and peak timing changes with site, formation, and rolling-window width. The 50 s boundary is retained because it lies within or near the later part of the broadly elevated early Hg–TOC interval, because Blue Lias profiles provide the clearest and most consistently shaped correlation structure around this interval, and because one shared cutoff permits direct comparison among sites. Similar broad structure in the 5, 10, and 20 s analyses supports treating HgLT as a broad early-release pool rather than selecting the boundary from one sharp correlation maximum. HgLT and HgHT are therefore used in place of the commonly utilized HgOMS/HgOTH terminology.

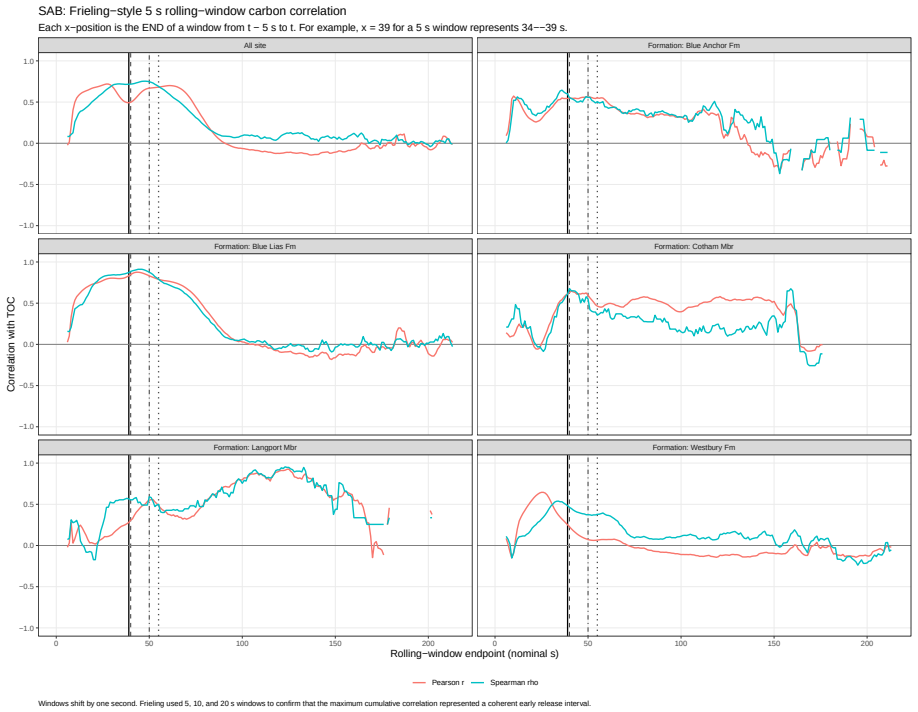

Figure 9: 5 second rolling window TOC correlations with Hg release for St Audries Bay.

4.2.2 CaCO3 correlations

Hg–$CaCO_3$ relationships are more heterogeneous than Hg–TOC relationships and vary among sites, formations, and portions of the TDP. Lavernock Point shows pronounced negative early Hg–$CaCO_3$ correlations at whole-site level and within several formations. St Audries Bay also contains several negative early relationships, but their timing and magnitude vary among formations. Wilkesley is the most variable of the three sites with $CaCO_3$ data: some intervals show negative relationships, whereas others are weak or positive, so $CaCO_3$ does not exert one consistent site-wide control. No rolling

Hg–$CaCO_3$ analysis was performed for Watchet because $CaCO_3$ data were unavailable for this site.

Strong negative Hg–$CaCO_3$ correlations are consistent with dilution of Hg-bearing phases by carbonate and/or covariance with lithology and facies. They are also considered here as another potential bounding site for Hg, particularly in low-TOC facies.

4.3 TDP characteristics

TDPs are shown as unit-area-normalized Hg release-rate profiles so that differences among curves reflect release shape rather than total Hg concentration. Each independent, duplicate-collapsed profile therefore contributes equally to the mean curves. The dashed 50 s line marks the operational HgLT–HgHT division. Across all four sites, most mean TDPs contain a major release feature within approximately the first 50 s, but the prominence of later shoulders and secondary release between approximately 50 and 100 s varies substantially. Median-profile checks preserve the same broad geometries, indicating that the mean patterns are not solely an artifact of a few extreme profiles.

4.3.1 Site-level TDP distributions

Figure 10 compares formations within each site. Wilkesley is generally dominated by an early peak at approximately 25–50 s. Westbury and Cotham profiles commonly contain relatively narrow, pronounced early peaks, whereas the much larger Blue Lias dataset shows greater sample-to-sample variability in peak position and the magnitude of the late-release tail; many Blue Lias profiles retain release through approximately 80–100 s. No Wilkesley Langport profile can be evaluated because no analyzed sample falls within the very thin member.

Watchet shows pronounced formation-level differences. The Westbury mean peaks broadly near the 50 s boundary, whereas Cotham profiles are substantially more heterogeneous and commonly show broad release from approximately 40 to 100 s. Langport profiles are also broad, with substantial release on both sides of 50 s. The Blue Lias returns to a comparatively narrow early-release shape with the principal peak before or close to 50 s. Interpretation of the Westbury mean is limited by its small sample size.

Lavernock Point shows a strong stratigraphic change in TDP shape. Westbury profiles are comparatively narrow, while Cotham and Langport profiles are broader and later, with much of the principal release occurring around or after 50 s and extending toward approximately 100 s. The Blue Lias returns to a pronounced early peak followed by a lower-amplitude tail. The Cotham and Langport therefore have a stronger late-release component than the equivalent Wilkesley profiles.

St Audries Bay contains the largest number of independent TDPs and substantial within-formation variability. Many profiles contain a pronounced early feature at approximately 25–40 s together with broader later release. Blue Anchor profiles commonly contain both an early peak and secondary release from approximately 60 to 100 s. Westbury profiles are dominated by an early peak but often retain a later shoulder or tail. Cotham and Langport profiles are particularly heterogeneous, ranging from strong early release to broad maxima later than 50 s. Blue Lias profiles generally retain a pronounced early peak but vary substantially in the magnitude and duration of the later tail. The mean site-level view can therefore resemble a two-component or double-peaked geometry at St Audries Bay, although in the Blue Lias the later component is more commonly a shoulder than a distinct second maximum.

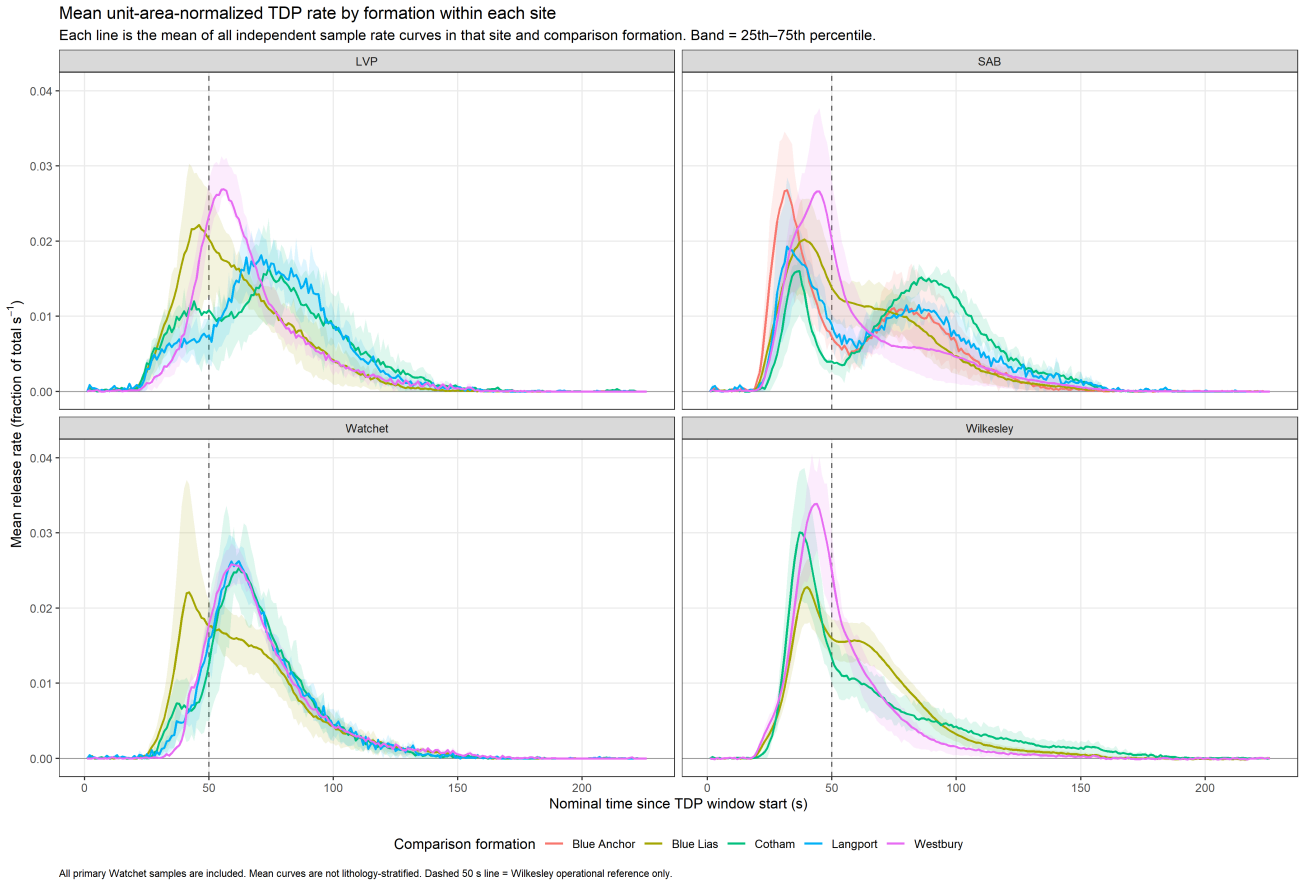

Figure 10: Mean unit-area-normalized TDPs by formation within each site.

4.3.2 Formation-level patterns

Mean TDP shape varies both among formations and among sites within the same formation (Figure 11). The Blue Lias shows the greatest qualitative cross-site similarity: at all four sites the principal mean release occurs in the early part of the TDP, generally before or close to 50 s, followed by a variable later shoulder or tail. Exact peak position, width, and post-50 s release still differ among sites, so the formation is similar in broad geometry rather than identical.

Westbury profiles also show some cross-site consistency but retain a geographic split in detailed shape. Wilkesley and St Audries Bay are dominated by relatively early release with smaller late shoulders, whereas Lavernock Point and Watchet have relatively later mean maxima. The Westbury is therefore somewhat more internally consistent than the Lilstock Formation, but not as coherent as the Blue Lias.

Cotham shows the strongest cross-site divergence. Wilkesley retains a comparatively sharp early-release peak, whereas Lavernock Point, St Audries Bay, and Watchet show broader release extending across and beyond the 50 s boundary. Several Cotham means therefore contain substantial release from approximately 50 to 100 s. Notably, Wilkesley and St Audries Bay can resemble one another more closely in broad Cotham geometry than either necessarily resembles a geographically nearer site, showing that distance alone does not control TDP similarity.

Langport profiles are also heterogeneous among the three sites with samples. Watchet contains a relatively prominent early component, whereas Lavernock Point and St Audries Bay show broader release extending substantially beyond 50 s. No Langport TDP is available from Wilkesley. Blue

Anchor is sampled only at St Audries Bay and therefore cannot be compared among sites; its mean contains a pronounced early peak and broad later release.

Overall, stratigraphically equivalent formations do not produce identical TDP shapes among sites. The strongest relative cross-site similarity occurs in the Blue Lias, whereas Cotham and Langport show substantially greater differences in peak timing and late-release behavior.

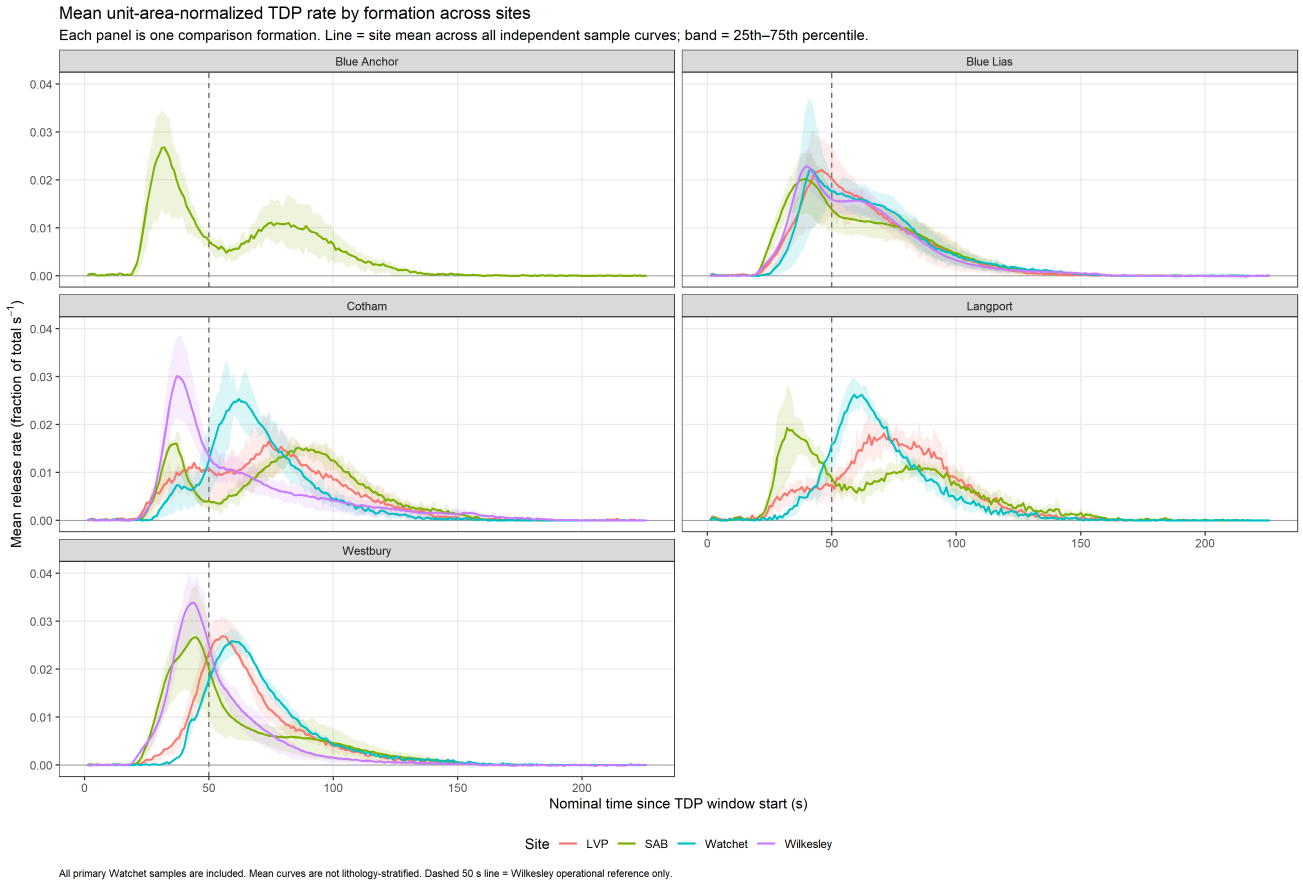

Figure 11: Mean unit-area-normalized TDP by formation across sites.

4.3.3 Lithological controls

The functional-lithology comparison groups samples as Carbonate, Mud-rich, and Sandstone, with mud-rich descriptions taking the principal label for mixed lithologies. TDP shape remains variable within each broad group (Figure 12.) Mud-rich profiles are the most similar in broad shape: their mean profiles tend toward a dominant single peak, latest at Watchet, somewhat earlier at Lavernock Point, and earliest at Wilkesley and St Audries Bay. Carbonate and Sandstone groups show less clear cross-site ordering, and Sandstone comparison is especially limited by small and uneven sample numbers. Site-to-site differences remain visible after lithologic grouping, so functional lithology alone does not explain the full range of TDP shapes.

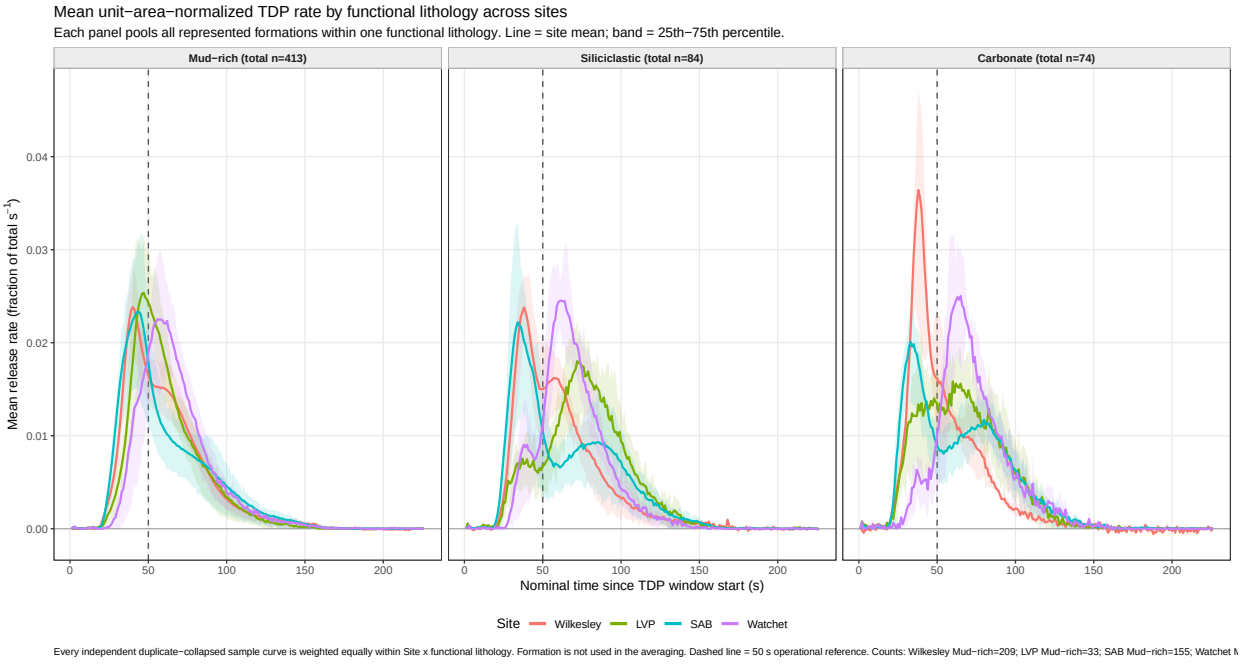

Figure 12: Mean unit-area-normalized TDP by functional lithology across sites.

Individual-profile (Figures 13 - 16)provide a complementary view of intra-unit lithologic variability. At Lavernock Point, Westbury, Cotham, and Blue Lias samples show TDP-shape changes associated with changes in functional lithology; the same pattern is present but less clear at St Audries Bay. These figures are retained as qualitative evidence that lithology here contributes to within-formation TDP variation without fully accounting for it.

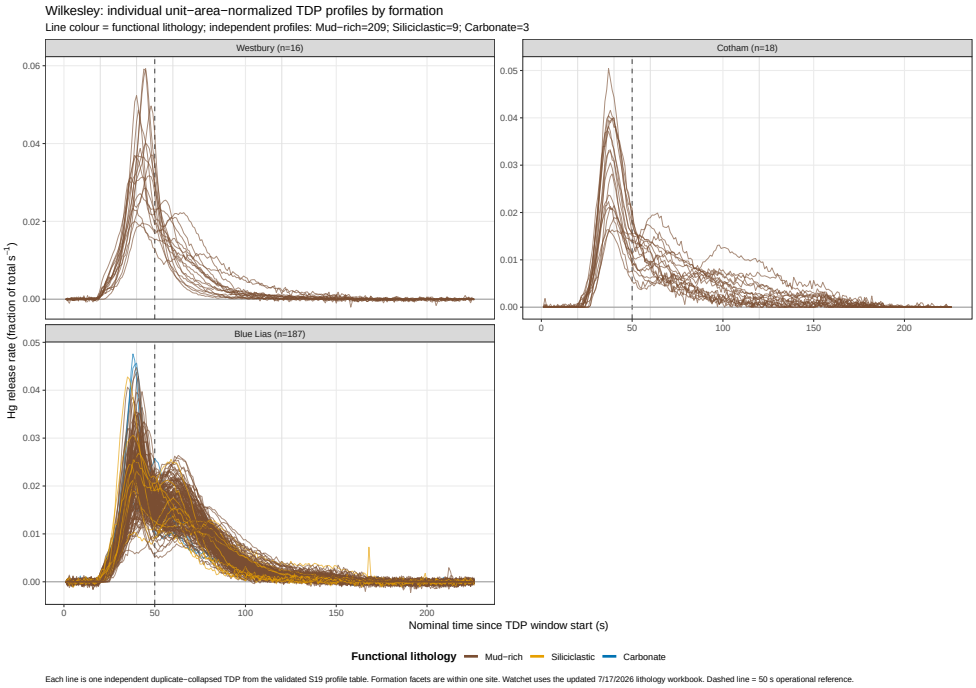

Figure 13: All individual +functional lithology TDPs by formation within Wilkesley borehole.

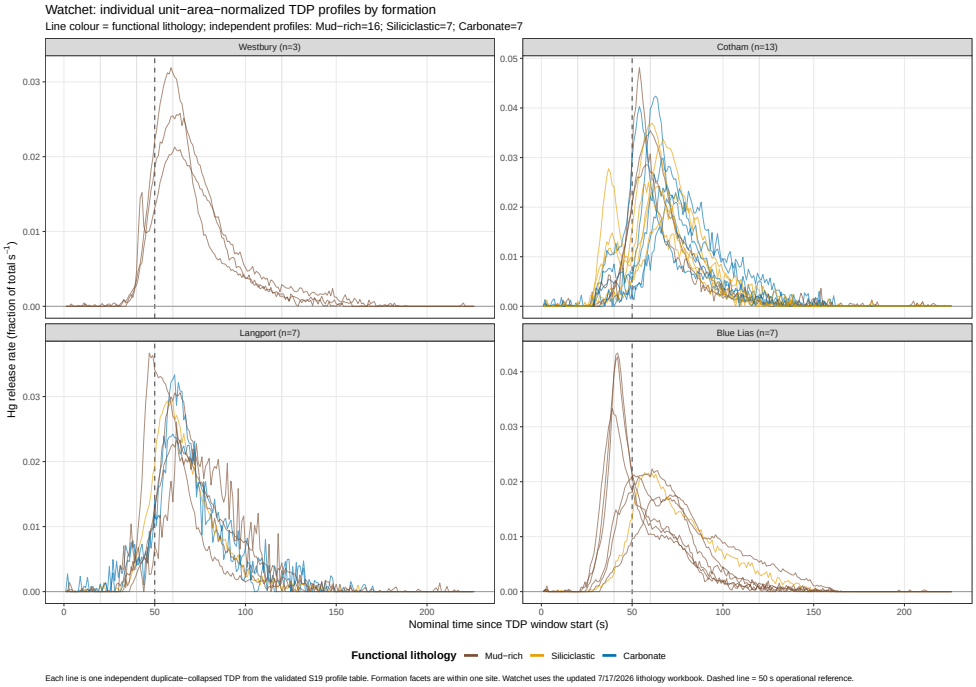

Figure 14: All individual TDPs by formation +functional lithology within the Watchet outcrop.

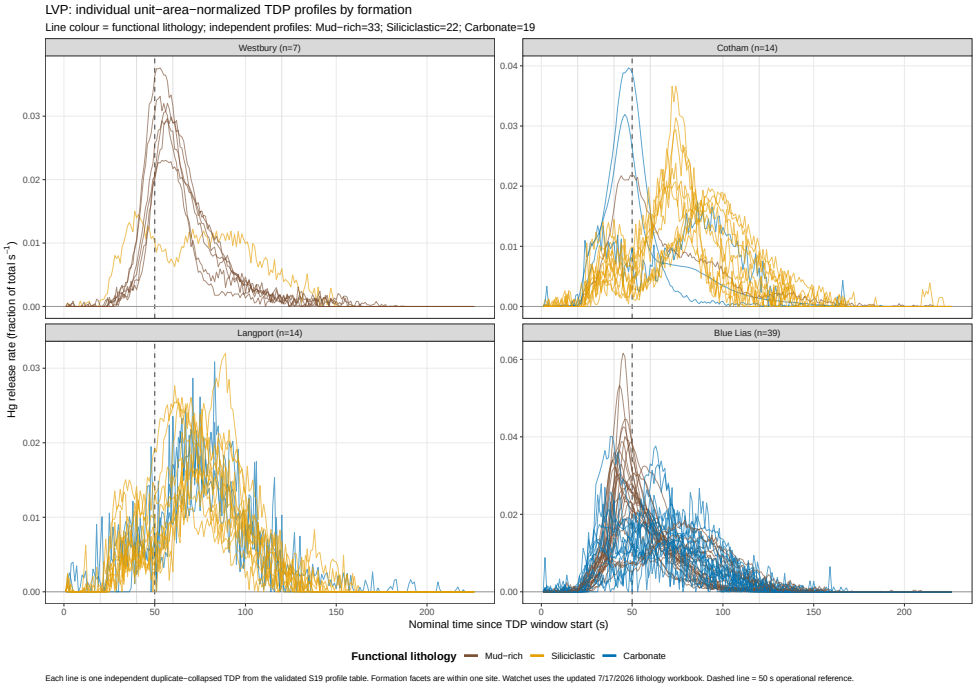

Figure 15: All individual TDPs by formation +functional lithology within Lavernock Point.

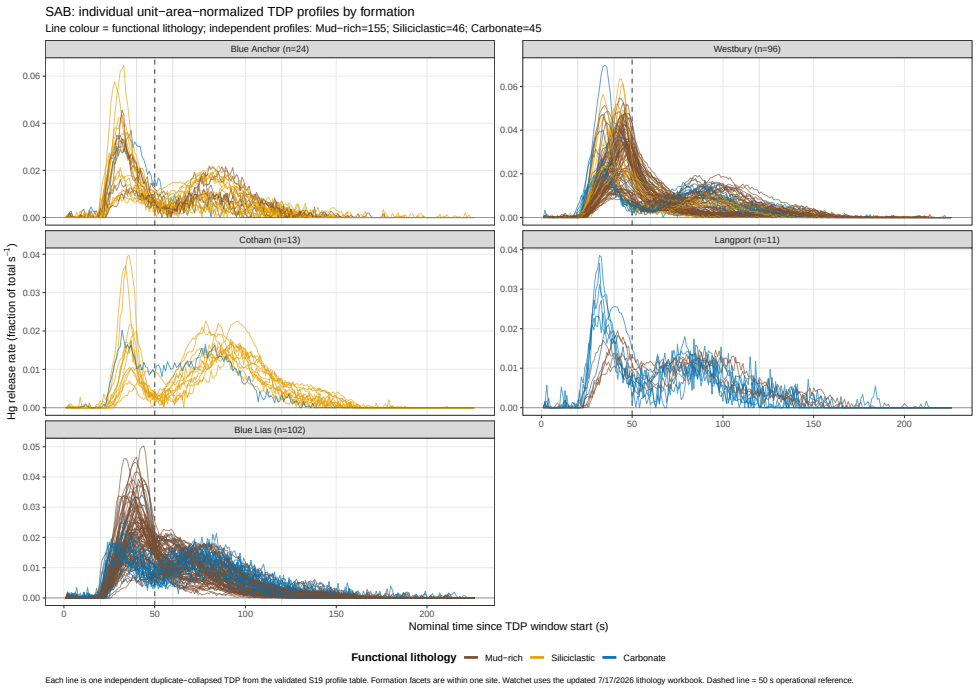

Figure 16: All individual TDPs by formation +functional lithology within St Audries Bay.

4.4 Associations between Hg fractions and potential host-phase proxies

Relationships between Hg and potential host-phase proxies vary substantially among sites and stratigraphic intervals.

4.4.1 Wilkesley

Wilkesley shows the weakest and most stratigraphically variable host-phase relationships. At whole-borehole scale, HgLT is only weakly associated with TOC, HgHT shows little relationship with TOC, and relationships with $CaCO_3$, Rb, Zr, and Rb/Zr are generally weak or inconsistent. Within individual formations, however, both the strength and direction of these relationships change substantially. For example, Hg–TOC relationships become negative in parts of the Westbury and Upper Hettangian, while Hg–$CaCO_3$ relationships can become positive in the Westbury. No single TOC, carbonate, or siliciclastic proxy therefore explains Hg behavior throughout the borehole.

4.4.2 Watchet

The Watchet host-phase analysis is limited to TOC because $CaCO_3$ data are unavailable. Within the Cotham Member, absolute HgT and HgLT show little consistent relationship with TOC, whereas the proportion of Hg released as HgLT increases with TOC. This suggests that organic matter may influence the partitioning of Hg between early and late release more strongly than total Hg concentration. This interpretation is limited by the small number of samples within individual formations.

4.4.3 Lavernock Point

Lavernock Point shows the clearest relationship between Hg and the available host-phase proxies. In the Blue Lias, HgT and particularly HgLT are strongly associated with TOC, whereas Hg concentrations are strongly negatively associated with $CaCO_3$. Similar positive Hg–TOC and negative Hg–$CaCO_3$ relationships occur in the Langport Member. The Cotham also retains a positive HgLT–TOC relationship, although carbonate relationships are weaker than in the overlying units. These patterns are consistent with strong organic-matter association combined with carbonate dilution and/or facies covariation.

4.4.4 St Audries Bay

St Audries Bay also shows strong but formation-dependent host-phase relationships. HgT and HgLT are strongly positively associated with TOC in the Blue Lias, while all Hg fractions are negatively related to $CaCO_3$. Positive Hg–TOC and negative Hg–$CaCO_3$ relationships also occur in the Westbury, Cotham, and Langport, although their strength varies among units and HgHT is generally less consistently related to TOC than HgLT. The Blue Anchor Formation shows weaker relationships overall.

Cross-site summary No single host-phase proxy explains Hg behavior across all four sites. Lavernock Point and St Audries Bay show the clearest positive Hg–TOC relationships and recurring negative Hg–$CaCO_3$ relationships, whereas Wilkesley is substantially more heterogeneous and Watchet is less well constrained. HgLT is generally more closely associated with TOC than HgHT, but this relationship is neither universal nor stratigraphically constant. These differences indicate that a single Hg/TOC normalization or whole-site host correction cannot be assumed to represent the sedimentary Hg receptor equally well in every interval.

4.5 Residual mercury across sites

The standard tanh–TOC correction substantially reduces portions of the broad Cotham enrichment visible in raw Hg/TOC records, but the residual records do not converge on one stratigraphically identical positive anomaly across all sites. Wilkesley, Lavernock Point, and St Audries Bay all lose much of the broad Cotham enrichment after host correction; the upper-Cotham Lavernock special-bed anomaly remains conspicuous. Watchet is less strongly constrained because of the smaller dataset and lack of matched inorganic host proxies.

The preservation-aware results are also site-specific. Wilkesley retains formation-specific relationships with TDP centroid, St Audries Bay retains formation-specific relationships with the early-release fraction, and Lavernock Point retains no additional TDP metric after the selected host model. Thus, the same model-selection sequence does not produce one transferable preservation term. The lack of a universal correction is itself a result: measurable TDP structure remains important in some sections but not others.

5 Discussion

5.1 Hg/TOC cohesion across sites

The four Hg/TOC records differ substantially in absolute magnitude and stratigraphic variability, but all contain enrichment within the Cotham Member. Wilkesley is comparatively ‘spiky’ throughout,

with a prominent Cotham enrichment and additional excursions in the Westbury and pre-*P. planorbis* Blue Lias. Watchet is also variable, with relatively high Hg/TOC concentrated in the middle and upper Cotham. Lavernock Point is comparatively flat through much of the section, with a modest elevation beginning in the Cotham and continuing into the lower Langport, plus one extreme upper-Cotham excursion associated with the microbialite-bearing special bed. The densely sampled basal Blue Lias at Lavernock does not contain a comparable Hg/TOC increase. St Audries Bay is relatively stable outside the main enrichment interval, with its clearest increase concentrated in the Cotham, particularly the middle of the member.

The recurrence of Cotham Hg/TOC enrichment at four geographically separated British sections supports the fidelity of Hg as a regional stratigraphic signal. Because the sites occupy different positions within the regional basin system and different distances from CAMP source regions, contemporaneous enrichment is consistent with a geographically widespread perturbation to the Hg cycle. The Cotham is also an unusual depositional interval, characterized by shallowing, exposure, renewed transgression, strong facies changes, carbonate development, and locally microbial facies. The next apparent question is therefore whether the recurrent Hg/TOC enrichment is driven primarily by external Hg loading or by a recurring change in the sedimentary receptor.

The exploratory Cotham residual-Hg/TDP test depicted in Figure 17 directly addresses this question by comparing the TDPs of relatively high Cotham residuals with the remaining Cotham samples within each site. The high subset is defined relative to each site's Cotham residual distribution. No single TDP geometry or functional lithology characterizes the upper-residual subset across all four sites. Lavernock Point is the clearest exception: its highest Cotham residuals have substantially earlier TDP centroids and larger early-release fractions, but this relationship is driven importantly by the special-bed cluster and includes both Carbonate and Mud-rich samples. Watchet shows a weaker tendency toward earlier release, whereas Wilkesley and St Audries Bay show little TDP separation. The figure therefore argues against a simple explanation in which the recurrent Cotham Hg/TOC signal is produced everywhere by one peculiar functional lithology or one common TDP receptor state. It does not, however, eliminate local depositional control, which is clearly important for the Lavernock Point "special bed". Additionally, Hg enrichment in the Cotham member could still be related to paleogeographic features of the Cotham even if it isn't driven by a change to the Hg-receptor system.

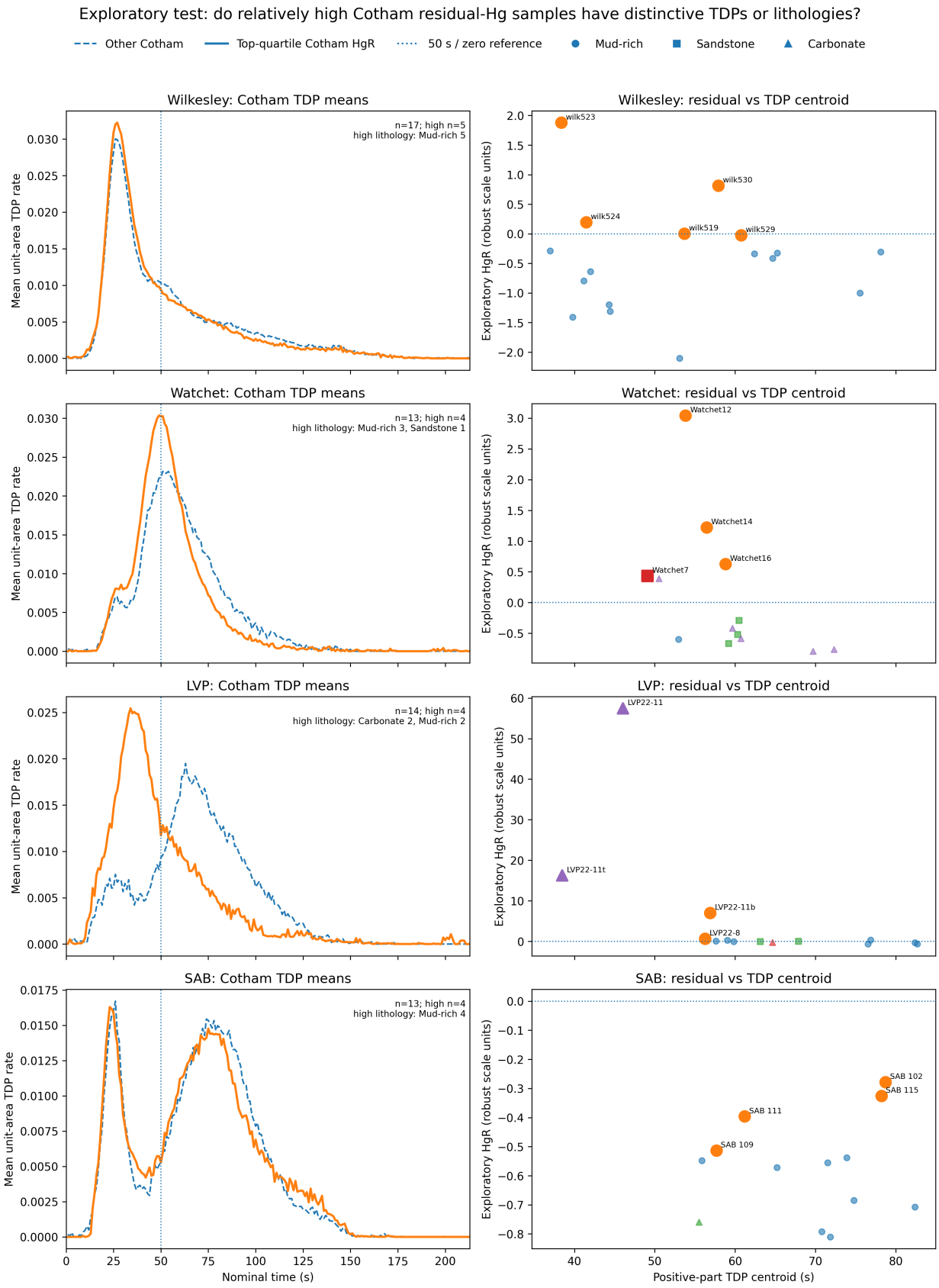

Figure 17: Exploratory comparison of Cotham Member residual Hg, TDP shape, and functional lithology across the four study sites.

A second important observation is that the apparent cross-site coherence in raw Hg/TOC is not preserved after host-based residual correction. Much of the broad Cotham enrichment is removed at Wilkesley, Lavernock Point, and St Audries Bay, while the Lavernock special-bed spike remains. The disappearance of an Hg/TOC peak after correction does not show that Hg deposition did not increase; it means that the enrichment cannot be separated cleanly from the modeled receptor using TOC alone. Wilkesley is particularly informative because its Cotham remains overwhelmingly mud-rich and lacks the same obvious lithologic shift seen at some Bristol Channel sites, yet its major Cotham Hg/TOC excursions are still largely removed by host correction. This argues against functional lithology alone as the explanation for the residual behavior.

One possible interpretation is that background Hg retention becomes limited by receptor abundance or receptor capacity in ways not captured by a simple ratio, producing apparent nonlinearity between Hg and TOC. The current data do not uniquely demonstrate such flux limitation, but the contrast between large Hg/TOC excursions and reduced residuals shows that the form of the Hg–TOC relationship matters. This is especially relevant at Wilkesley, where the raw record is much more variable than at the other sites. That variability is not readily explained by sampling resolution alone: St Audries Bay is sampled at similarly high or higher density in parts of the section but does not reproduce the same degree of Hg/TOC scatter. The combined linear, nonlinear, TDP, and rolling-$CaCO_3$ results therefore point toward a Wilkesley-specific receptor or basin-history control. Possible contributors include clay-mineral transformation, burial history, organic-matter character, or other basin-specific processes.

5.2 Limitations to residual Hg for British T–J sections

Residual-Hg approaches attempt to distinguish changes in external Hg loading from variation caused by the sedimentary Hg-receptor system. Their usefulness therefore depends strongly on how well the background Hg–host relationship can be defined. Two assumptions are particularly important. First, the section must contain a sufficiently large background interval so that ordinary Hg behavior can be distinguished from anomalous enrichment. Second, that background should represent a relatively consistent depositional system, such that the fitted relationship is not averaging across major changes in lithology, host-phase abundance, redox conditions, or other controls on Hg retention.

These conditions are more readily satisfied in long, comparatively homogeneous records like the Mochras core, where extended intervals of broadly similar mud-rich sediment provide a more internally consistent background for defining Hg–host relationships (Fendley et al., 2024). The British T–J sections studied here are more complicated. The Westbury, Cotham, Langport, and Blue Lias represent substantial changes in water depth, carbonate production, organic matter, lithology, and depositional environment over relatively short stratigraphic intervals. The TDP results independently show that the Hg receptor changes across these transitions: equivalent formations do not always produce equivalent TDP shapes, and particularly large cross-site differences occur within the Cotham and Langport. A single whole-site Hg–TOC relationship therefore combines several different depositional and receptor states rather than defining one uniform background.

This limitation helps explain why the standard residual records do not preserve the apparent cross-site coherence seen in raw Hg/TOC. Much of the broad Cotham enrichment is reduced after correction for the modeled HgLT–TOC relationship. This does not demonstrate that Hg deposition did not increase during the Cotham. Instead, it shows that the enrichment cannot be separated confidently from the modeled background when that background itself spans substantial changes in the sedimentary receptor. The resulting residuals are consequently sensitive to how the background interval and functional relationship are defined.

A second limitation is that the sedimentary receptor is not completely characterized by TOC. Hg can

also be associated with sulfide, clay-mineral, and other phases, while carbonate and siliciclastic input can alter concentrations through dilution or facies covariation. Sample-matched sulfur data are not available across all four sections at sufficient resolution, and proxies such as Rb/Zr and functional lithology do not uniquely identify specific clay or sulfide hosts. The absence of a remaining relationship with TOC or $CaCO_3$ therefore does not establish that the final residual is independent of the sedimentary receptor.

Residual Hg is consequently most defensible where a long and internally consistent background interval is available and where major changes in the depositional system are limited or explicitly modeled. In rapidly changing successions such as these British T–J sections, residual-Hg analysis remains useful as a diagnostic tool, but quantitative interpretation of residual magnitude as excess volcanic Hg requires stronger validation of the background receptor. Candidate volcanic signals should therefore be evaluated together with stratigraphic correlation, TDP behavior, lithology, host-phase indicators, carbon-isotope stratigraphy, and independent evidence for CAMP activity.

5.3 Insights gained from TDPs

The rolling Hg–TOC correlations show that organic-carbon association is generally strongest during the early part of the TDP. This supports using the 50 s boundary as a common operational split for comparison, but the timing and strength of the association vary among sites and formations. The cutoff is therefore less distinct in some low-TOC intervals, whereas the relatively organic-rich Blue Lias produces the most consistently interpretable rolling-correlation geometry. More organic-rich facies also tend to contain a stronger early-release component, consistent with the general HgLT–TOC relationship.

TDP shape changes systematically through the studied successions. The Blue Lias shows the greatest cross-site similarity, generally with an early principal peak and variable late shoulder, whereas Cotham and Langport show much greater differences in peak position, width, release after 50 s, and prominence of later components. One plausible depositional explanation is that the more consistently marine, deeper-water Blue Lias provided a more stable sedimentary receptor than the strongly fluctuating shallow-water Lilstock facies. Several simple statistical alternatives are insufficient by themselves to explain this: median profiles retain the same broad shapes as the means, and Watchet would not be expected to show the same Blue Lias cross-site consistency if consistency was only a product ofthe high number of samples from the Blue Lias. Sample size may contribute to apparent smoothness, but it does not fully explain the formation pattern.

Substantial variability also occurs among samples within the same formation and within the same functional lithology. Stratigraphic equivalence therefore does not guarantee an identical Hg-receptor system. This is particularly important for Cotham and Langport, where depositional environment changes rapidly and mean TDPs differ strongly among sites.

TDPs also provide an independent diagnostic of whether conventional Hg–host correction has fully described the background. If residual Hg still varies systematically with TDP shape, then the residual remains related to a measurable property of the receptor. This occurs at Wilkesley, where centroid relationships are retained, and at St Audries Bay, where early-release fraction retains explanatory information. It does not occur at Lavernock Point after the selected host model. This suggest that the residuals for these sites are not independent of diagenetic and sedimentary Hg-receptor effects that have been demonstrated to influence TDP shape: early TDP releases were linked to higher HgT and HgLT residuals once correlation with TOC had been accounted for.

The principal value of TDPs in paleovolcanic studies may therefore be diagnostic rather than mineral-specific. A bulk Hg or Hg/TOC excursion identifies a change in abundance, whereas a TDP tests whether the character of the measured Hg pool changed at the same time. An excursion without a

substantial TDP change is less obviously associated with a major change in the measured receptor; an excursion accompanied by a large TDP shift requires greater caution because enrichment and receptor change coincide. The substantial stratigraphic and cross-site variation observed here shows that this receptor is not constant and explains why HgLT/TOC alone is not sufficient for all intervals in this dataset.

5.4 A possible clay-transformation control on early Hg release

Patterns in the shape of these TDPs, particularly the existence of early and late peaks, may offer evidence to move TDP shape closer to a mineralogic cause.

An empirical study found that as geologic samples thermally mature in the lab, their Hg release happens later on average, reducing the HgLT component (Indraswari et al., 2025). One possible mechanism for the pronounced early-release component involves expandable clay minerals and clay–organic associations during thermal desorption. Mud-rich samples commonly contain strong early release, initially suggesting that HgLT might be preferentially associated with high-surface-area clay minerals such as smectite. Work by Kongchum and others reported positive Hg–smectite relationships in modern sediments, with an $r = 0.538$ between clay minerals and Hg, and smectite being the only correlated clay mineral (2011). The large loss of specific surface area expected as expandable smectite-rich material becomes more illitic—approximately 500–800 $m^2\,g^{-1}$ for smectite versus roughly 30–100 $m^2\,g^{-1}$ for illite alters the capacity of clays to retain organic matter and by extension Hg (Bergaya et al., 2006).

Preliminary fractionation by Krishnaswamy showed that dispersion with Calgon strongly separated the early-release Hg peak from the later-release component. Because Calgon disperses fine clay particles and disrupts aggregation, this result is consistent with HgLT being associated with a dispersible clay-rich or clay–organic fraction. The fractionation result therefore strongly links HgLT to the dispersible fraction.

Expandable clays are relevant because their interlayers and surface properties change during burial and heating. Geological smectite-to-illite transformation begins at comparatively low diagenetic temperatures and involves dehydration, interlayer reorganization, and progressive loss of expandability. These changes provide a mechanism by which Hg associated with clay surfaces, interlayers, or clay-bound organic matter could become mobilized. During a Lumex run, the sample is heated rapidly through temperatures at which expandable clays can dehydrate and structurally modify. This temperature range is roughly 80–110 °C in sedimentary basins (Hower et al., 1976). The early TDP peak could therefore partly represent Hg liberated as an expandable clay–organic receptor changes during analysis.

However, rapid dry heating in the Lumex can not be equated with the complete burial-diagenetic smectite-to-illite reaction, which depends on time, water, potassium availability, temperature, and other poorly understood constraints. The more conservative interpretation is that low-temperature dehydration, interlayer collapse, or related structural modification of expandable clay–organic associations may account for HgLT release.

6 Conclusions

1. Hg/TOC enrichment recurs within the Cotham Member at all four studied British Rhaetian–Hettangian sections, although its magnitude and detailed stratigraphic expression vary among sites. Importantly, the samples associated with this enrichment do not share a consistent TDP geometry or functional lithology across the four sections. This argues against the excursion being generated simply by the pronounced shallowing, facies shifts, or lithologic changes that characterize the Cotham Member. Instead, the recurrence of Hg enrichment across multiple depositional

settings, without a common change in the Hg-receptor system, supports an externally forced perturbation to the Hg cycle.

2. Residual-Hg approaches are most useful where the background Hg–host relationship can be defined from a sufficiently long and internally consistent background interval. This requires enough non-anomalous samples and relatively limited change in the depositional system, so that the modeled relationship is not being fit across major shifts in lithology or Hg-receptor behavior, which other analysis has shown to effect the Hg interpretations. The Mochras core, where long intervals of broadly similar mud-rich lithology provide a more stable background, are therefore better suited to residual-Hg analysis than rapidly changing successions such as the British T–J sections studied here. Where background intervals are short or depositional conditions change substantially through the section, residuals become strongly dependent on how the background is defined and are less defensible as quantitative estimates of excess volcanic Hg.

3. TDPs show that the Hg-receptor system changes through stratigraphy in ways that are not captured by bulk Hg concentration, Hg/TOC, or broad lithologic classification alone. Equivalent functional lithologies can display different TDP shapes among sites and formations, indicating that receptor behavior reflects more than lithology alone. The greatest cross-site similarity occurs in the Blue Lias, where relatively consistent marine depositional conditions are accompanied by broadly similar early-release TDP geometries. In contrast, the more environmentally variable Cotham and Langport intervals show substantially greater cross-site differences. This pattern suggests that depositional environment is an important control on the Hg-receptor system and that TDPs can reveal changes in receptor behavior that would otherwise remain unresolved.

4. More broadly, this novel synthesis of four sections from the Cheshire and Bristol Channel basins shows both the value and the limitations of sedimentary Hg as a paleovolcanism proxy. Repeated Hg enrichment across multiple sections can provide evidence for a regional perturbation to the Hg cycle, but the magnitude and preservation of that signal depend strongly on local depositional setting, Hg hosting, and post-depositional history. Sedimentary Hg is therefore most robust when interpreted across multiple sites and basin settings rather than from a single section, and when bulk Hg records are evaluated together with TDP behavior, host-phase proxies, stratigraphy, and independent evidence for volcanism. Quantitative reconstruction of volcanic Hg or carbon flux as was derived from the Mochras core requires an additional step: demonstration that the sedimentary receptor has been sufficiently constrained for the residual Hg signal to be interpreted independently of local sedimentary controls.

7 References

Bergaya, F., Theng, B. K. G., & Lagaly, G. (Eds.). (2006). *Handbook of clay science* (Vol. 1). Elsevier.

Bian, L., Chappaz, A., Wang, X., Amouroux, D., Schovsbo, N. H., Zheng, X., & Sanei, H. (2024). Improving mercury systematics with molybdenum and vanadium enrichments: New insights from the Cambrian–Ordovician boundary. *Geophysical Research Letters, 51*(8), Article e2023GL107188. https://doi.org/10.1029/2023GL107188

Blackburn, T. J., Olsen, P. E., Bowring, S. A., McLean, N. M., Kent, D. V., Puffer, J., McHone, G., Rasbury, E. T., & Et-Touhami, M. (2013). Zircon U–Pb geochronology links the end-Triassic extinction with the Central Atlantic Magmatic Province. *Science, 340*(6135), 941–945. https://doi.org/10.1126/science.1234204

Bond, D. P. G., & Grasby, S. E. (2017). On the causes of mass extinctions. *Palaeogeography, Palaeoclimatology, Palaeoecology, 478*, 3–29. https://doi.org/10.1016/j.palaeo.2016.11.005

Bos, R., Zheng, W., Lindström, S., Sanei, H., Waajen, I., Fendley, I. M., Mather, T. A., Wang, Y., Rohovec, J., Navrátil, T., Sluijs, A., & van de Schootbrugge, B. (2024). Climate-forced Hg-remobilization associated with fern mutagenesis in the aftermath of the end-Triassic extinction. *Nature Communications, 15*, Article 3596. https://doi.org/10.1038/s41467-024-47922-0

Capriolo, M., Mills, B. J. W., Newton, R. J., Dal Corso, J., Dunhill, A. M., Wignall, P. B., & Marzoli, A. (2022). Anthropogenic-scale CO_2 degassing from the Central Atlantic Magmatic Province as a driver of the end-Triassic mass extinction. *Global and Planetary Change, 209*, Article 103731. https://doi.org/10.1016/j.gloplacha.2021.103731

Clapham, M. E., & Renne, P. R. (2019). Flood basalts and mass extinctions. *Annual Review of Earth and Planetary Sciences, 47*, 275–303. https://doi.org/10.1146/annurev-earth-053018-060136

Cornford, C. (1986). The Bristol Channel Graben: Organic geochemical limits on subsidence and speculation on the origin of inversion. *Proceedings of the Ussher Society, 6*, 360–367.

Davies, W. (2025). *Exploring depositional and volcanic controls on sedimentary mercury concentrations across the Triassic–Jurassic mass extinction* [Unpublished report].

Davies, J. H. F. L., Marzoli, A., Bertrand, H., Youbi, N., Ernesto, M., & Schaltegger, U. (2017). End-Triassic mass extinction started by intrusive CAMP activity. *Nature Communications, 8*, Article 15596. https://doi.org/10.1038/ncomms15596

Fendley, I. M., Frieling, J., Mather, T. A., Ruhl, M., Hesselbo, S. P., & Jenkyns, H. C. (2024). Early Jurassic large igneous province carbon emissions constrained by sedimentary mercury. *Nature Geoscience, 17*(3), 241–248. https://doi.org/10.1038/s41561-024-01378-5

Fox, C. P., Holman, A. I., Rigo, M., Al Suwaidi, A., & Grice, K. (2022). Paleowildfire at the end-Triassic mass extinction: Smoke or fire? *Global and Planetary Change, 218*, Article 103974. https://doi.org/10.1016/j.gloplacha.2022.103974

Frieling, J., Fendley, I. M., Nawaz, M. A., & Mather, T. A. (2024). Assessment of Hg speciation changes in the sedimentary rock record from thermal desorption characteristics. *Geochemistry, Geophysics, Geosystems, 25*(4), Article e2024GC011502. https://doi.org/10.1029/2024GC011502

Greene, S. E., Martindale, R. C., Ritterbush, K. A., Bottjer, D. J., Corsetti, F. A., & Berelson, W. M. (2012). Recognising ocean acidification in deep time: An evaluation of the evidence for acidification across the Triassic–Jurassic boundary. *Earth-Science Reviews, 113*(1–2), 72–93. https://doi.org/10.1016/j.earscirev.2012.03.009

Guest, T. (2025). *Mercury and the End-Triassic mass extinction: Exploring environmental, depositional and volcanic controls on mercury speciation* [Master's thesis, University of Oxford].

Hautmann, M., Benton, M. J., & Tomašových, A. (2008). Catastrophic ocean acidification at the Triassic–Jurassic boundary. *Neues Jahrbuch für Geologie und Paläontologie – Abhandlungen, 249*(1), 119–127.

https://doi.org/10.1127/0077-7749/2008/0249-0119

Hesselbo, S. P., Robinson, S. A., Surlyk, F., & Piasecki, S. (2002). Terrestrial and marine extinction at the Triassic–Jurassic boundary synchronized with major carbon-cycle perturbation: A link to initiation of massive volcanism? *Geology, 30*(3), 251–254. https://doi.org/10.1130/0091-7613(2002)030<0251:TAMEAT>2.0.CO;2

Hesselbo, S. P., Robinson, S. A., & Surlyk, F. (2004). Sea-level change and facies development across potential Triassic–Jurassic boundary horizons, SW Britain. *Journal of the Geological Society, 161*(3), 365–379. https://doi.org/10.1144/0016-764904-069

Hower, J., Eslinger, E. V., Hower, M. E., & Perry, E. A., Jr. (1976). Mechanism of burial metamorphism of argillaceous sediment: 1. Mineralogical and chemical evidence. *Geological Society of America Bulletin, 87*(5), 725–737. https://doi.org/10.1130/0016-7606(1976)87<725:MOBMOA>2.0.CO;2

Indraswari, A. O., Frieling, J., Mather, T. A., Dickson, A. J., Jenkyns, H. C., & Idiz, E. (2024). Investigating the behavior of sedimentary mercury (Hg) during burial-related thermal maturation. *Geochemistry, Geophysics, Geosystems, 25*(6), Article e2024GC011555. https://doi.org/10.1029/2024GC011555

Indraswari, A. O., Frieling, J., Idiz, E., Mather, T. A., Jenkyns, H. C., Robinson, S. A., & Dickson, A. J. (2025). Limited mercury (Hg) partitioning into bitumen and efficient gaseous Hg reabsorption during early thermal maturation of organic-rich mudrocks. *Geochimica et Cosmochimica Acta, 403*, 240–251. https://doi.org/10.1016/j.gca.2025.07.001

Jiskra, M., Heimbürger-Boavida, L.-E., Desgranges, M.-M., Petrova, M. V., Dufour, A., Ferreira-Araujo, B., Masbou, J., Chmeleff, J., Thyssen, M., Point, D., & Sonke, J. E. (2021). Mercury stable isotopes constrain atmospheric sources to the ocean. *Nature, 597*(7878), 678–682. https://doi.org/10.1038/s41586-021-03859-8

Kaiho, K., Tanaka, D., Richoz, S., Jones, D. S., Saito, R., Kameyama, D., Ikeda, M., Takahashi, S., Aftabuzzaman, M., & Fujibayashi, M. (2022). Volcanic temperature changes modulated volatile release and climate fluctuations at the end-Triassic mass extinction. *Earth and Planetary Science Letters, 579*, Article 117364. https://doi.org/10.1016/j.epsl.2021.117364

Knoll, A. H., & Follows, M. J. (2016). A bottom-up perspective on ecosystem change in Mesozoic oceans. *Proceedings of the Royal Society B: Biological Sciences, 283*(1841), Article 20161755. https://doi.org/10.1098/rspb.2016.1755

Kongchum, M., Hudnall, W. H., & DeLaune, R. D. (2011). Relationship between sediment clay minerals and total mercury. *Journal of Environmental Science and Health, Part A, 46*(5), 534–539. https://doi.org/10.1080/10934529.2011.551745

Krishnaswamy, K., Frieling, J., Percival, L. M. E., Littler, K., Reboulet, S., Fendley, I. M., Mather, T. A., & Robinson, S. A. (2026). Minimal perturbation of the global mercury cycle by the Paraná–Etendeka Large Igneous Province (PE–LIP) during the onset of the Valanginian Weissert Event. *Geochemistry, Geophysics, Geosystems, 27*(7), Article e2026GC012969. https://doi.org/10.1029/2026GC012969

Lindström, S. (2016). Palynofloral patterns of terrestrial ecosystem change during the end-Triassic event: A review. *Geological Magazine, 153*(2), 223–251. https://doi.org/10.1017/S0016756815000552

Lindström, S., van de Schootbrugge, B., Hansen, K. H., Pedersen, G. K., Alsen, P., Thibault, N., Dybkjær, K., Bjerrum, C. J., & Nielsen, L. H. (2017). A new correlation of Triassic–Jurassic boundary successions in NW Europe, Nevada and Peru, and the Central Atlantic Magmatic Province: A time-line for the end-Triassic mass extinction. *Palaeogeography, Palaeoclimatology, Palaeoecology, 478*, 80–102. https://doi.org/10.1016/j.palaeo.2016.12.025

Liu, Z., Tian, H., Yin, R., Chen, D., & Gai, H. (2022). Mercury loss and isotope fractionation during thermal maturation of organic-rich mudrocks. *Chemical Geology, 612*, Article 121144. https://doi.org/10.1016/j.chemgeo.2022.121144

Lyman, S. N., Cheng, I., Gratz, L. E., Weiss-Penzias, P., & Zhang, L. (2020). An updated review of atmospheric mercury. *Science of the Total Environment, 707*, Article 135575. https://doi.org/10.1016/j.

scitotenv.2019.135575

Marzoli, A., Bertrand, H., Knight, K. B., Cirilli, S., Buratti, N., Vérati, C., Nomade, S., Renne, P. R., Youbi, N., Martini, R., Allenbach, K., Neuwerth, R., Rapaille, C., Zaninetti, L., & Bellieni, G. (2004). Synchrony of the Central Atlantic magmatic province and the Triassic–Jurassic boundary climatic and biotic crisis. *Geology, 32*(11), 973–976. https://doi.org/10.1130/G20652.1

Pantazopoulou, A. (2023). *Volcanism and mass extinctions: Are these signals reproducible? A geochemical and petrological examination of the Triassic–Jurassic Boundary of South Wales, U.K.* [Unpublished honours undergraduate thesis]. University of Oxford.

Plant, J. A., Jones, D. G., & Haslam, H. W. (Eds.). (1999). *The Cheshire Basin: Basin evolution, fluid movement and mineral resources in a Permo-Triassic rift setting.* British Geological Survey.

Raup, D. M., & Sepkoski, J. J., Jr. (1982). Mass extinctions in the marine fossil record. *Science, 215*(4539), 1501–1503. https://doi.org/10.1126/science.215.4539.1501

Richoz, S., van de Schootbrugge, B., Pross, J., Püttmann, W., Quan, T. M., Lindström, S., Heunisch, C., Fiebig, J., Maquil, R., Schouten, S., Hauzenberger, C. A., & Wignall, P. B. (2012). Hydrogen sulphide poisoning of shallow seas following the end-Triassic extinction. *Nature Geoscience, 5*(9), 662–667. https://doi.org/10.1038/ngeo1539

Ruhl, M., & Kürschner, W. M. (2011). Multiple phases of carbon cycle disturbance from large igneous province formation at the Triassic–Jurassic transition. *Geology, 39*(5), 431–434. https://doi.org/10.1130/G31680.1

Shen, J., Feng, Q., Algeo, T. J., Liu, J., Zhou, C., Wei, W., Liu, J., Them, T. R., Gill, B. C., & Chen, J. (2020). Sedimentary host phases of mercury (Hg) and implications for use of Hg as a volcanic proxy. *Earth and Planetary Science Letters, 543*, Article 116333. https://doi.org/10.1016/j.epsl.2020.116333

Singh, P., Lu, W., Lu, Z., Jost, A. B., Lau, K., Bachan, A., van de Schootbrugge, B., & Payne, J. L. (2023). Reduction in animal abundance and oxygen availability during and after the end-Triassic mass extinction. *Geobiology, 21*(2), 175–192. https://doi.org/10.1111/gbi.12533

Stow, M., Dickson, A. J., Prytulak, J., Dellinger, M., Alcock, V., Hesselbo, S. P., Nowell, G. M., & Hilton, R. G. (2026). Rhenium isotopes reveal enhanced rock organic carbon oxidation over the Toarcian Oceanic Anoxic Event. *Nature Communications, 17*, Article 5303. https://doi.org/10.1038/s41467-026-71533-6

Torsvik, T. H., & Cocks, L. R. M. (2017). *Earth history and palaeogeography.* Cambridge University Press. https://doi.org/10.1017/9781316225523

Ullmann, C. V., Damaschke, M., Hesselbo, S. P., Jiang, M., Lawrence, K., Leng, M. J., Mattioli, E., Bancalin, J., Page, K. N., Pudal, N., Ruhl, M., & Silva, R. L. (2026). An integrated biostratigraphy and chemostratigraphy for the dawn of the Jurassic (the Hettangian stage in the Cheshire Basin, UK). *Journal of Earth Science, 37*(3), 945–967. https://doi.org/10.1007/s12583-025-0205-6